Noncontact 3D Biological Shape Measurement from Multiple Views

Youmei Ge

A thesis submitted for the degree of Master of Science

The University of Western Australia
Department of Computer Science

May 1994

Abstract

Many clinically important applications require measurements on a large portion of the human body surface that may not be visible from a single view. For example, a single view may be insufficient for the measurement of a complete facial surface for facial plastic surgery. And observing breast surfaces from multiple views is needed in accurate breast volume measurement. On the other hand, most 3D vision systems only recover 3D data from a single viewpoint, and the recovered 3D data are often incomplete due to the occlusion problem and thus cannot uniquely define the surface. A unique and more complete description of the surface is necessary for most applications such as measuring area or volume and finding the best 3D registration between corresponding surfaces.

This thesis describes a structured light based system for fast and noncontact 3D measurement of the human body from multiple views. A particular application of our system is the study of human lactation through measuring the breast surface and volume. Fast, accurate, non-contact, and biologically safe measurement is the key requirement in our application. We use structured light to fulfill the requirement. Based on the SHAPE system [4,3], a single view structured light system developed at Monash University, our system for breast volume measurement generates more complete 3D information on object surfaces by observing the object from more than one viewpoint. The breast volume is computed using the integrated data from all views.

We present a simple method that performs 3D measurement from multiple views simultaneously. Combined with a camera and a projector, a mirror is used in

the method to create an additional viewpoint to recover the occluded regions that are illuminated by the light source but were previously invisible to the camera. Images from the two views, one directly seen by the camera and the other seen via the mirror, are taken simultaneously. We develop the method for the purpose of achieving more complete measurements without increasing image capture time, which is very useful in situations where both speed and accuracy are important.

The complete 3D description of the surface of objects requires the acquisition of several images from different vantage viewpoints. Each image contains information on the part of the object that is visible from its viewpoint. A very important task consists in the integration of the information present in each view. We have developed a two view system to achieve a more complete breast volume measurement. The system uses a stationary sensor at each view. Our system can largely eliminate the occlusion regions produced by a single view system, and all data from different views are integrated into an object-centered coordinate system and resampled by a single parametric grid. The system has been used to accurately measure short-term changes in breast volume for lactating mothers. Currently, the system is also used to observe the breast volume change of pregnant women over many weeks' time.

Preface

Much of the work presented here has been published. The method of combining a mirror with an active sensor presented in Chapter 3 was published in the *Proceedings of the 1992 Department Research Conference* [28].

The work of the two view system for breast volume measurement presented in Chapter 4 was published in the *Proceedings of First Australian and New Zealand Conference on Intelligent Information System 1993* [29].

This thesis describes greater details of our work, expands on previous publications, and provides further improvements that have been made.

Acknowledgements

This thesis would not be possible without various forms of support from many people. In particular, I would like to thank my supervisor, Associate Professor Robyn Owens, for her inspiration, guidance and encouragement throughout the course of this research work, and to Associate Professor Peter Hartmann for his inspiration, advice and support.

I am grateful to Peter Kovesi for his advice, to Laurie McKeaig for his technical support, to Jacqueline Kent, David Cox and Steven Daly for their assistance in the experiments, to Wilfred Brewster for constructing equipment, and to many members in the Robvis research group for their interests and suggestions.

I thank Dr Kim Ng at Monash University for sending me the papers of his related work.

My thanks also go to all the mothers and babies who have participated in the experiments for this work.

This research was funded by the NH&MRC and ARC grants.

Finally, I would like to thank my parents for their love, patience and understanding over the years, and my husband, Hong Xie, for his love and constant support.

Contents

Abstract i

Preface iii

Acknowledgements iv

1 Introduction 1

1.1 Optical 3D Measurement Techniques 2

1.1.1 Triangulation-based Stereo 3

1.1.2 Time of Flight 9

1.2 3D Measurement of Human Body Surfaces 10

1.2.1 Methods by Contact 10

1.2.2 Stereophotogrammetry 11

1.2.3 Structured Light 12

1.3 Our System 13

1.4 Outline of the Thesis 15

2 Breast Volume Measurement for Lactating Mothers 16

2.1 Introduction 16

2.2 A Moiré Topography Approach 19
2.2.1 The Definition of Breast Volume 19
2.2.2 Positioning 20
2.2.3 Summary 20
2.3 A Structured Light System 21
2.3.1 Breast Boundary Detection 21
2.3.2 Data Smoothing and Pruning 22
2.3.3 Volume Calculation 22
2.3.4 Summary 22
2.4 The Occlusion Problem 23
2.4.1 Linear Interpolation 23
2.4.2 Bivariate Quadratic Surface Fitting 24
2.4.3 Accuracy of Volume Estimation with Occluded Regions . . . 25
2.5 Conclusion 28

3 Recovering Occluded Regions from Mirror Images 30

3.1 Introduction 30
3.2 A Virtual Viewpoint via a Mirror 32
3.2.1 System Geometry 32
3.2.2 Virtual Object Measurement 34
3.2.3 From Virtual Object to Real Object 36
3.3 Implementation 37
3.3.1 Mirror Calibration 38

3.3.2 Reconstruction from Mirror Images 38
3.4 Experimental Results 39
3.5 Discussion 39
3.6 Conclusion 41

4 3D Shape Measurement from Multiple Views 47

4.1 Introduction 47
4.2 System Arrangement 52
4.3 Calibration and Triangulation 53
4.4 Surface Resampling 54
4.5 Breast Volume Estimation 61
4.6 Experimental Results 62
4.6.1 Experiments of Breast Models 64
4.6.2 Experiments of Human Breasts 64
4.7 Discussion 69
4.8 Conclusion 69

5 Conclusion 71

A The SHAPE System 74

A.1 Introduction 74
A.2 Overview of the SHAPE System 76
A.2.1 Stripe Location 77
A.2.2 Stripe Coding 77

A.2.3 Triangulation and Calibration 78

A.3 Accuracy 81

Bibliography **83**

List of Figures

1.1 Simple geometry for stereopsis. 4

1.2 Camera-centered active triangulation geometry. 5

2.1 An example of a human breast surface with an occluded region: (a) the front view; (b) the side view. 24

2.2 A breast surface displayed in front (a) (c) (e) and side view (b) (d) (f) with the approximated surface patch to the occluded region: (a)-(b) by the linear interpolation; (c)-(d) by the bivariate quadratic surface fitting; (e)-(f) the real shape. 26

2.3 Breast shapes:
(a) bowl-shaped:
the anterior projection is smaller than the radius of the circumference;
(b) hemispherical:
the anterior projection is equal to the radius of the circumference;
(c) conical:
the anterior projection is greater than the radius of the circumference;
(d) dependent:
the papillae are pointing downwards. 27

2.4 An example of a breast surface with different occluded regions before (a) and after feeding (b). 28

3.1 Camera, projector and mirror geometry. 33

3.2 A pencil of planes. 35

3.3 Relations between the plane of a mirror and the planes of a pair of real and virtual light. 37

3.4 The field of view of a camera and a projector with a mirror. 40

3.5 A breast model: (a) the grey level image showing both real scene and virtual scene; (b) the measurement of the real object, rotated by 10°. 43

3.6 A breast model: (c) the measurement of the virtual object; (d) the result by merging (c) and Figure 3.5 (b), rotated by 10°. 44

3.7 A coffee mug: (a) the grey level image showing both real scene and virtual scene; (b) the measurement of the real object, rotated by 30°. 45

3.8 A coffee mug: (c) the measurement of the virtual object; (d) the result by merging (c) and Figure 3.7 (b), rotated by 30°. 46

4.1 Geometry of two camera and projector pairs. 52

4.2 A display of a breast model at the first viewpoint: (a) the intensity image; (b) the 3D sample data. 55

4.3 A display of a breast model at the second viewpoint: (a) the intensity image; (b) the 3D sample data. 56

4.4 Surface segments. 57

4.5 Combined data from the first and the second viewpoint. 57

4.6 Breast-centered coordinate system. 59

4.7 A cone model surface represented by triangular facets. 60

4.8 Result of the breast model by surface resampling. 61

4.9 Triangular pyramid volume elements. 63

4.10 The relationship between the volume of milk removed by the infant at a breast-feed, measured by test weighing (abscissa), and the change in breast volume, measured by the two view system (ordinate). . . 66

A.1 Camera and projector arrangement in the SHAPE system. 75

A.2 An example of a point display of measured 3D data. 76

A.3 Coding patterns. 79

A.4 Active triangulation geometry. 80

List of Tables

4.1 Results of the volume measurement on the breast model (ml). . . . 65

4.2 The averaged statistical data of 30 sections generated by the CBM system and the two view system. 67

4.3 Results of the breast surface measurement of Mother A. 67

4.4 Results of the breast surface measurement of Mother B. 68

4.5 Results of the breast surface measurement of Mother C. 68

Chapter 1

Introduction

Medical imaging techniques have been in wide use for viewing of 3D structure within the human body. Such techniques include magnetic resonance imaging and computed tomography [71]. However, there remains an unfilled biomedical need for 3D measurement of surfaces on the human body. There are many important biomedical problems requiring rapid, accurate, noncontact, and safe measurement of human body surfaces.

In facial plastic surgery [74], accurate measurement of facial surfaces can assist both surgeons and patients to plan and evaluate facial changes before and after the surgery. For women with breast cancer and facing mastectomy, recovering the outer appearance of the removed breast requires three dimensional information on the breast, e.g. size, shape, and volume. Breast volume measurements are also required in the biochemical study of human lactation. An accurate measurement of the breast surface and volume has the potential to be an important tool in the study of biochemical control of milk synthesis in breast feeding women [34,22]. In burn area measurement, an accurate area measurement is important for computing fluid replacement, caloric requirement, and dosimetry of burn therapeutic agents [78,54].

Conventional measurement systems by contact methods or using mechanical devices have shortcomings in terms of accuracy, safety, speed, and cost. Measurement

methods by contact generally require contacting (and possibly depressing) the skin which is not biologically safe. For example, in burn area measurement, any contact with damaged skin can carry a high risk of infection, and in breast surface and volume measurement, mechanical contact deforms the surface, producing measurement errors.

The work of this thesis is on the development of an accurate and non-contact measurement system for the 3D measurement of the human body surface using optical rangefinding techniques. In particular, the system is applied to the biochemical study of human lactation by measuring breast surface and volume of lactating women.

We begin this chapter by surveying optical rangefinding techniques in 3D sensing which have been developed for a variety of applications, including biomedical applications and industrial inspection tasks. Next we describe some of the previous work in 3D measurement of human body surfaces, examining in detail three main methods employed in the area: measurement methods by contact, stereophotogrammetry, and structured light. We then discuss the occlusion problem in active vision systems. Finally we close the chapter with an overview of our system and an outline of the thesis.

1.1 Optical 3D Measurement Techniques

A *range image* is a large collection of distance measurements from a known reference coordinate system to surface points on object(s) in a scene. A *range-imaging sensor* is any combination of hardware and software capable of producing a range image of a real world scene under appropriate operating conditions [11]. Optical range imaging or 3D measurement systems collect 3D information from visible object surfaces in a scene. These systems can be used to guide various processes such as robotic manipulation, automatic inspection, and medical diagnosis.

Human beings use a number of depth cues to infer 3D structure, including tex-

ture, contours, shading, stereo, motion, and focus. Machine vision "structure-from-X" modules have been designed using each of these clues. The machine vision techniques coming into practical use today for directly recovering range data are based on two principles: triangulation or time of flight. In this section, we survey these two major types of optical range finding methods with concentration on the triangulation-based methods.

1.1.1 Triangulation-based Stereo

The process of inferring depth (or other geometric information about the surface of 3D objects) using two or more images acquired from different viewpoints, in human or machine vision, is called *stereo*. *Triangulation* is the procedure by which an object point can be located in three dimensions from its two camera images as the intersection of the known lines of sight. Triangulation-based stereo methods can be classified as passive (using ambient light only) and active (using controlled illumination). An important advantage of stereo over most of the other methods is that no prior assumptions about statistics, surface reflectivity, or 3D shape are needed. We survey three popular triangulation-based stereo methods: passive stereo, active stereo using structured lighting, and Moiré interferometry.

Passive Stereo

Range from passive stereo is one of the functions of the human visual system. Since it uses natural illumination and performs well in humans, passive stereo is an attractive method of 3D sensing.

A typical passive sensing technique is stereopsis where 3D information is extracted by matching features of the images taken from different viewpoints. Figure 1.1 illustrates a basic arrangement for stereopsis [36] in which the optical axes of two cameras are parallel and separated by a distance b. In parallel axis stereo, depth can be computed directly from disparity as $z = bf/d$, where z is the distance from the common baseline to the object along the direction parallel to the optical axis,

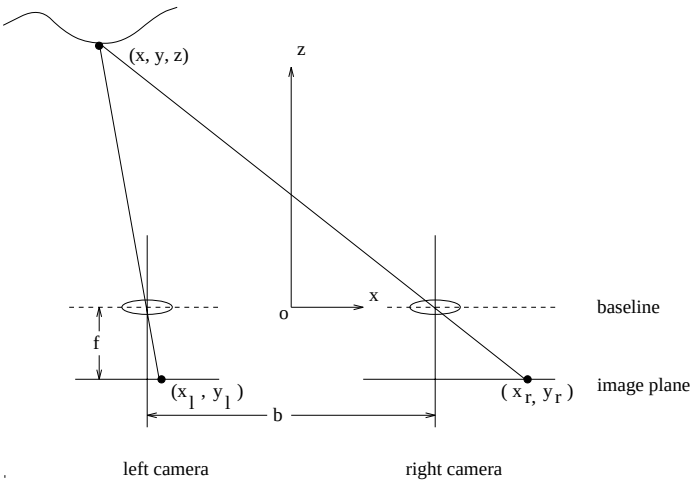

Figure 1.1: Simple geometry for stereopsis.

f is the focal length, and d is the disparity, which is the difference in the left and right x-axis image coordinates, $x_l - x_r$. The origin of the system of the two cameras is taken to be the midpoint between the two optical centers.

We see that distance is inversely proportional to disparity, which itself is directly proportional to the baseline. Thus, given a fixed error in determining the disparity, the accuracy of the depth determination increases with increasing baseline.

The stereo correspondence problem is to find matching pairs of features in two images which are images of the same physical feature in the scene. Solving the stereo correspondence is the most difficult problem in passive stereo and the key to any working machine stereo system. It requires sufficient visual information at the matching features to establish a unique correspondence. Stereo matching can be classified into area-based and feature-based methods. Area-based methods [46,80] may chose pixels as the matching primitive and matching is performed using correlation between the intensity values in two dimensional neighborhoods (e.g. small rectangular patches) of the candidate pixels from the left and right camera images. Feature-based methods [51,8] generally use high-order features such as edges, linked edge contours and line junctions as matching primitives. More methods for stereo matching are reported in [62].

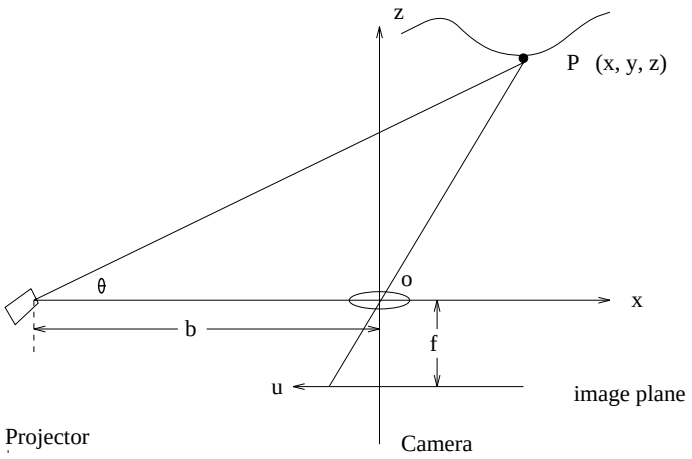

Figure 1.2: Camera-centered active triangulation geometry.

Active Stereo Using Structured Light

Structured light is a form of stereo where one of the passive cameras is replaced by an "active camera" or light source which projects known patterns onto the scene. Images of the known patterns are recorded using a single camera. The light patterns in the camera images appear distorted due to the curvature of the object. By locating the features of the light patterns on the camera images and matching them correctly to the projected patterns, the three-dimensional positions of points on the object surface can be determined by triangulations.

A simple geometry of an active triangulation system is shown in Figure 1.2. A single camera is aligned with the center of the lens located at the origin and the optical axis parallel to the z-axis. A light projector is located along the negative x-axis at a baseline distance b from the origin. The projector illuminates the object with a light beam at an angle θ relative to the x-axis baseline. The 3D coordinates of the point $P(x, y, z)$ can be determined by triangulation [11]: $x = bu/(f \cot\theta - u)$, $y = bv/(f \cot\theta - u)$, and $z = bf/(f \cot\theta - u)$ where f is the focal length of the camera and (u, v) is the image coordinate of the point P.

Various forms of structured light may be projected onto a scene, including points, lines, a grid pattern, and a coded binary pattern.

A point active sensor illuminates the object with a single light beam which forms a light spot on the object surface. The projected beam periodically scans the object in raster fashion and the angle of the projected beam with respect to the baseline can be determined by timing. Rioux [67] has developed a synchronized laser point scanner in which the projection and the detection of a laser beam are both scanned using a single rotating polygonal mirror. Some point scanning systems are discussed by Gerhardt and Kwak [31], and Besl [11].

A line active sensor illuminates the object with a sheet of light which forms a light stripe on the object surface. The light stripe appears curved in the camera image. By computing the intersection of the ray from each pixel of the stripe image with the projected plane of light, 3D information can be extracted on the illuminated portions of the object surface. An entire contour of the surface can be obtained by scanning the plane of light over the object in the direction orthogonal to the light plane. Mirrors [70,66] or turntables [42,68] can be used as scanning devices.

By projecting a full two-dimensional grid pattern onto the scene, range measurements can be performed from a single projected grid image. Thus the data acquisition rate can be increased, but at the cost of having to solve the correspondence problem for structured light, often referred to as the *grid labeling problem.* The grid labeling problem involves correctly matching detected features in the camera image with the corresponding features in the projected grid pattern. Constraints may be imposed on the surface shapes in solving the grid labeling problem, otherwise ambiguities can arise. Hall *et al.* [32] describe a grid pattern method for obtaining sparse range images of simple objects. Stockman and Hu [76] have examined the ambiguity problem using relaxation labeling. Grid pattern based rangefinding systems are also discussed by Keizer [44] and Blake *et al.* [13].

Space encoding is used in solving the grid labeling problem by projecting a sequence of coded binary patterns in which a given feature is either present (on) or not present (off) in each of the sequence numbers. By assigning a unique binary number to each feature, N features can be uniquely labeled from projected patterns $\lceil \log_2 N \rceil$ where $\lceil x \rceil$ represents the least integer $\geq x$. Potsdamer and Altschuler [60] describe a nu-

merical stereo camera consisting of a laser and electro-optic shutter synchronized to a camera using standard binary patterns. Vuylsteke and Oosterlinck [77] have developed another binary coding scheme. They project a specially formulated binary mask in which each local neighborhood of the mask has its own signature. Alexander and Ng [4] describe a shape measurement system using a liquid crystal light valve mounted in a projector to code an array of 64 horizontally projected stripes. A single camera views the scene from above the projector. Identification of each light stripe in the camera image via the coding process allows triangulation as in the normal line sensors. Appendix A describes the system in detail. Space encoding techniques do not need a scanning mechanism and thus lower the image acquisition time. The ambiguities in the grid labeling problem may not arise by using coded binary patterns.

The main advantages of the active binocular method are its simplicity and low costs, making it the most common technique in many applications. The active illumination can be a disadvantage in natural environments and even in industrial environments where specular reflections can be a problem. There is also the problem of lack of data due to view constraints on both the camera and the light source. We discuss the problems in detail in the following section.

Moiré Interferometry

Moiré interferometry is the technique whereby depth information can be inferred from Moiré fringe patterns. A Moiré pattern is defined as the low spatial frequency interference pattern created when two gratings with regularly spaced patterns of higher spatial frequency are superimposed on one another [11].

The essence of the technique is that the object surface under measurement is illuminated with a light source passing through a linear optical grating and the scene is viewed by a camera from a different direction through an identical grating. Thus, Moiré fringe contour patterns are formed which appear as dark and light stripes on the camera image. Depth information is generated by analysing the patterns.

Moiré interferometry is a form of active triangulation using structured light. It offers the potential for inexpensive, fast, and accurate range imaging [7] for smooth object surfaces. The main problem of the method is that ambiguities can arise in identifying fringe patterns. Depth discontinuities on object surfaces may cause the fringe order to be lost due to a disparity jump of more than one fringe.

Occlusion Problems

The Occlusion problem or the missing data problem in binocular active vision systems is that no accurate information can be obtained in the occluded areas which are invisible to both or either of the camera and the light source. The problem can result in unmeasurable parts on the surface to be measured, and thus a lack of completeness for an overall measurement.

There are two sources of missing data areas on the object surface. One is caused by sensor viewing constraints. A single view may not be sufficient for certain applications and thus measurements from multiple viewpoints are needed. Creating a multiple view sensor may involve either the motion of the scene (objects) or the motion of the sensors. One common method based on scene motion is to use a turntable [69,42,68] to rotate the object so that the surface patches at multiple viewpoints can be measured. In the methods based on sensor motion, one approach is to maneuver a single sensor around a stationary object with a robot. The other is to use multiple sensors (camera/projector pairs) in different viewpoints to capture the appropriate views [74]. A given application of ranging systems may combine any scene motion with any sensor motion to achieve its goals. More details about various multiple view vision systems are described in Chapter 3 and Chapter 4.

The other type of missing data areas comes from specular reflection problems. These areas cannot reflect a reasonable amount of light to be detected by the camera. Techniques based on structured lighting require that the surface of the object reflect a reasonable amount of light diffusely so that the illuminated spot or stripe on the camera image can be precisely detected. This is an ideal condition that

cannot be met in practice, and variations in surface reflectance generate errors in the range measurement. The relation between reflectance variation and range error in the case of a single ray is discussed by Mundy and Porter [55]. For example, a very black surface area would not reflect much light and a highly mirrored surface area would not reflect much light diffusely. Although these areas can be measured by means of enhancement of the image intensity, or by adjusting the camera's aperture, they are difficult to measure when the areas of extreme white and black are present simultaneously. In the case of measurement of a human face for biomedical applications, the eyes and eyebrows are often the missing data areas due to their low reflectivity compared with the other parts of the face. This is also observed when measuring a large sized breast surface, the missing data areas are often at the base and lower sides of the breast surface due to their inconsistent lighting reflection with the other parts of the surface. The requirement of consistent surface reflection may be a limitation of all structured illumination methods. The missing data areas resulting from inconsistent surface reflection can occur even in multiple view systems. Surface representation techniques can be used to model these missing data areas which involve the generation of a complete surface representation using a set of control points on the surface. Various methods for three dimensional surface representation and reconstruction are discussed by Bolle and Vemuri [15].

1.1.2 Time of Flight

Range may be measured by the time of flight ranging apparatus which are classified as ultrasonic range finders and laser range fingers [41]. When a short ultrasonic pulse or a laser beam is transmitted towards an object, some of its energy is reflected back to the transmitter. If the time interval between the transmitted and received signal is measured, the distance between the source and the object can be obtained.

Basically, there are two laser range finder designs: continuous wave and pulsed. Continuous wave range finders [57,10] emit a continuous, either amplitude-modulated or frequency-modulated, signal during the time that range is being measured. Pulsed range finders [47,41] emit short pulses, wait for an echo, and use the transit

time to determine range.

Time of flight range finders directly measure range data. No image processing is involved, nor are assumptions concerning the shapes of measured objects. Moreover, time of flight range finders eliminate the occlusion problem encountered in all triangulation based methods with nonzero baseline separation, and thus can generate more complete range data. The main disadvantage of time of flight techniques is their high cost. In addition to this, laser range finders may not be biologically safe to use in measuring human bodies for biomedical applications.

1.2 3D Measurement of Human Body Surfaces

In this section, previous systems for 3D shape measurement of human body surfaces are surveyed. We concentrate on three main approaches that are widely used for measuring 3D shape of human surfaces: methods by contact, stereophotogrammetry, and structured lighting.

1.2.1 Methods by Contact

Milles *et al.* [52] describe a measurement system using mechanical devices. They have developed an electromechanical instrument called the facial plethysmograph to measure facial volume. The instrument uses a mobile feeler arm with a wheel that rolls over the facial surface in a horizontal plane. The position of the feeler arm in each of two orthogonal directions is sensed using mechanical to electrical transducers (Linear Variable Differential Transformers, or LVDTs). The electrical signals from the LVDTs are used to drive an X-Y plotter which records the contour that is the intersection of a horizontal plane with the facial surface. From a number of such uniformly spaced contours, facial volumes may be computed by standard numerical integration methods.

Hall *et al.* [33] review various methods for normal physical measurements. Usual

methods for measuring breast volume include water displacement [39] or using a special breast measuring cylinder of plexiglass [33].

Measurement methods by contact generally require contacting (and possibly depressing) the skin, which is not biologically safe. For example, in burn area measurement, any contact with damaged skin can carry a high risk of infection, and in breast surface and volume measurement, mechanical contact deforms the surface, producing measurement errors. Moreover, data acquisition can be very time consuming.

1.2.2 Stereophotogrammetry

Stereophotogrammetry is one of the noncontact techniques used in the 3D measurement of human body surfaces. Stereophotogrammetric techniques generally involve taking a stereo pair of photographs. Three dimensional information on the surface of the measured object is generated by analysing the photographs using analytic plotters. Mollard *et al.* [53] have developed such a photogrammetric device to measure the human body for establishing the relationship between overall and segmentary dimensions, surfaces, and body volumes and evaluating the variability of these parameters. The system is composed of one pair of cameras and two vertical mirrors. The skin of the human subject is first marked with a series of 107 anatomical points in order to collect 3D data and calculate anthropometric dimensions, surfaces, and body volumes. The photographs taken by the stereo pair of cameras are then processed on an analytic stereo-plotter to generate the 3D information on the surface. Similar stereophotogrammetric techniques are also employed by Dixon and Newton [25] to measure cleft deformities, by Bullock and Harley [17] to measure 3D movement of human bodies and by Loopuyt and Blaustein [48] to acquire facial data for the design of safety masks.

The technique of stereophotogrammetry is capable of producing accurate and noncontact measurement of the human body surface, particularly allowing the measurement of predetermined anatomical points. However, it may suffer from two

defects: the cost of the stereoplotting equipment and the difficulties in establishing correspondence between the pair of photographs.

1.2.3 Structured Light

Many applications of non-contact human body measurements benefit from the use of biologically safe structured light. Such applications include the measurement of the human trunk shape for detection of deformations of the spinal column, the measurement of the human body size and surface shape for the garment manufacturing industry, the measurement of human body surface area and volume for clinical problems such as facial plastic surgery, burn areas, and breast reconstruction following mastectomy.

Frobin *et al.* [27] present a method for automatic evaluation of rasterstereographs of the human back. Based on the symmetry of the human body, they use a perpendicular stereo base. A set of parallel raster light beams are projected onto the human surface, and the raster lines are oriented horizontally. Any raster line feature on the camera image corresponds to a point on the appropriate line in the raster slide. Three dimensional information is obtained by establishing the correspondence between the features of the raster lines on the camera image and the positions of the raster lines in the raster slide.

Jones *et al.* [42] have developed an anthropometric shadow scanner to measure human body size and surface shape. The subject being measured is placed on a turntable and rotated through 360 degrees in measured angular increments. Four narrow stripes of light are projected from four banks of four special light sources to fall on the body in vertical planes. The whole scene is viewed by two banks of seven television cameras. The light planes are arranged to pass through the center of rotation of the turntable and the cameras are aligned so that some known point at the light slit edge of the field of view coincides with the center of rotation of the turntable. The system arrangement allows them to measure a body in terms of radii and angles in conjunction with heights in cylindrical coordinates. The

data acquisition time for a mannikin is about 3 minutes. One of the applications of the system is in the garment manufacturing industry and CAD applications in clothing technology. The other is in breast surgery for women with breast cancer and facing mastectomy. In order to restore the outer appearance of the removed breast, the system is used to calculate the volume of the removed breast tissue by pre-operative scanning of the breast surface. The volume data is then sent to a prosthetics manufacturer so that the true shape and the form of the removed breast can be made into a prosthesis that is a good fit.

Keizer [44] has developed a structured light system for fast noncontact 3D measurement of human body surface area and volume. The system can reconstruct the visible surface from a single camera image, and thus may be useful in situations where acquisition time is important. Keizer has also implemented both automatic and interactive methods for 3D registration of a smooth surface and a method of measuring volumes by summations of the volumes of elementary tetrahedra. The structured light system has been used to measure the surface area of burns and the volume of facial swelling.

Structured light has been used in a variety of biomedical applications for measurement of smooth and structureless surfaces of irregular shape. It is inherently noncontact, generally accurate, and biologically safe.

1.3 Our System

Many clinically important applications require measurements on a large portion of the human body surface that may not be visible from a single view. On the other hand, most 3D vision systems only recover 3D data from a single viewpoint, and the recovered 3D data are often incomplete due to the occlusion problem and thus cannot uniquely define the surface. A unique and complete description of the surface is necessary for most applications such as measuring area or volume and finding the best 3D registration between corresponding surfaces.

This thesis describes a structured light based system for fast and noncontact 3D measurement of the human body surface and volume from multiple views. A particular application of our system is the study of human lactation through measuring the breast surface and volume. Fast, accurate, non-contact, and biologically safe measurement is the key requirement in our application. We use structured light to fulfill the requirement. Based on the SHAPE system [4,3], a single view structured light system developed at Monash University, our system reconstructs the surface from more than one viewpoint and generates more complete 3D information on object surfaces.

We present a simple method that performs 3D measurement from multiple views simultaneously. Combined with a camera and a projector, a mirror is used in the method to create an additional viewpoint to recover the occluded regions that are illuminated by the light source but were previously invisible to the camera. Images from the two views, one directly seen by the camera and the other seen via the mirror, are taken simultaneously. We develop the method for the purpose of achieving more complete measurements without increasing time, which is very useful in situations where both speed and accuracy are important.

We have also developed a two view system for breast volume measurement. The system uses a stationary sensor at each view. The complete 3D description of the surface of objects requires the acquisition of several images from different vantage viewpoints. Each image contains information on the part of the object that is visible from its viewpoint. A very important task consists in the integration of the information present in each view. Our system can largely eliminate the occlusion regions produced by a single view system, and all data from different views are integrated into an object-centered coordinate system and resampled by a single parametric grid. The system has been used to accurately measure short-term changes in breast volume for lactating mothers. Currently, the system is also used to observe the breast volume change of pregnant women over many weeks' time.

1.4 Outline of the Thesis

We introduce the background of measuring breast volume for biochemical study of human lactation in Chapter 2. Human breast feeding is a very complex interaction between a mother and her infant. We survey the usual measurements of milk production and discuss the problems encountered in previous work.

Chapter 3 describes in detail the method of acquiring images from multiple views simultaneously. A mirror is used in our method as a virtual camera/projector pair to provide more information from a virtual viewpoint.

The implementation of the two view system for measuring breast surface and volume is described in Chapter 4. We review various approaches of 3D model construction from multiple views and present an approach to recover a smooth surface from 3D data obtained from different viewpoints. In addition, we demonstrate a method for estimating the change in volume of the 3D space.

Chapter 5 concludes with a critical assessment of the successes and limitations of our system, and some suggestions for further development.

Appendix A provides an overview of the SHAPE system. The system uses biologically safe structured white light, and recovers 3D data on the object surface by active triangulation using a camera/projector pair. With its high accuracy and image capture time of less than one second, the SHAPE system is very useful in biomedical applications for fast, noncontact and accurate measurement. The system is employed in the work of this thesis.

Chapter 2

Breast Volume Measurement for Lactating Mothers

Computer vision techniques have been widely used in biological applications. The Computerized Breast Measurement (CBM) system [38,4], based on active vision methods, has been developed to measure the rates of milk synthesis from the short-term changes in breast volume for lactating mothers. This chapter introduces the background of biochemical study of human lactation, describes the vision techniques employed in the system, and discusses problems encountered.

2.1 Introduction

An essential characteristic of mammals is the capacity of the female to nourish her infant with milk, the secretion of mammary glands. In almost all species the supply of milk is essential for the survival of the young. Recent research has shown that breast milk not only provides the infant with a source of nourishment for physical growth but also plays an important role in protecting the infant against disease as well as influencing the infant's digestion, metabolism and behaviour [56,34].

Human breast feeding is a very complex interaction between a mother and her infant. It is now generally recognized that during established lactation it is the infant's

appetite rather than the mother's capacity to synthesize milk that determines the level of milk production [63]. However, exactly how milk supply (rate of milk synthesis) is matched to demand (infant appetite) remains unknown [22]. The usual measurement of milk production by measuring the milk intake of the infant determines the infant's appetite rather than the mother's capacity to synthesize milk. Moreover, this may result in a major clinical problem: if a baby has the problem of failure to thrive, we do not have any tests to determine whether the problem is the mother's inability to synthesize enough milk for the baby, or the baby's inability to consume a sufficient amount of the milk available [34]. Therefore, investigations of biochemical factors controlling the synthesis of breast milk have required the development of a method that measures the short-term rates of milk synthesis in lactating women.

Authur *et al.* [5,7] have established the feasibility of using breast volume measurements to determine short-term rates of milk synthesis in lactating mothers. Authur *et al.* [7] obtain a close correlation between the change in breast volume before and after a breast feed and the volume of milk removed by the infant. Thus, it is suggested that an increase in the volume of the breast, over short periods of time (hourly), reflect an increase in the volume of milk retained within the breast. Consequently, the rate of short-term milk synthesis can be determined by the rate of change in the volume of the breast.

Measurement of milk production by test weighing [79,6] depends upon the infant's intake of milk at each individual feed which in turn depends upon the appetite of the infant at that time. Therefore, measurement of the rate of milk synthesis by determining the infant's intake has to be averaged over 24 hours [35], and cannot distinguish between the ability of the mother to synthesize milk and the infant's ability to consume the milk available. The technique of measuring the change in breast volume allows determination of breast milk synthesis over short periods of time independent of the direct influence of the infant's appetite. Recent research [22,23] has demonstrated that the measurement of short-term changes in breast volume has the potential to be an important tool in the study of biochemical control

of milk synthesis in women breast feeding their babies on demand.

A variety of conventional methods may be used to measure the breast volume; these include [33]:

- using a water-filled container placed over the breast and into which the breast is placed. Since the volume of water in the container is known, the breast size can be calculated from the water displaced;
- making a cast of the breast, and measuring the volume of the breast from the cast;
- measuring the breast size with a special breast measuring cylinder of plexiglass with a fitted domed piston and a scale, from which the breast size can be read.

Speed and accuracy are the important considerations when attempting to measure small increases in breast volume with time after breast feeding. The conventional measurement methods above have three drawbacks in measuring short-term changes in breast volume. First, these methods are based on manual operations. The accuracy of these methods cannot be guaranteed due to errors caused by the manual operations. Second, with these methods, the process of the measurement can be very slow, and thus may also affect the measurement accuracy since the breast volume is changing during the process of the measurement. Finally, all the methods above involve skin contact which not only affects accuracy but also is invasive to the mother. They may be suitable for breast volume measurement for non-lactating women, but of limited practical use for lactating mothers.

It has been observed [7] that a consistent pose must be adopted by the mother at each measurement phase, as any movement of the skin would alter the relative contribution of the chest wall to breast volume. Furthermore, inspiration and expiration would also change the measured volume by changing the contribution of the chest wall to the volume measurement. Therefore, fast, accurate, non-invasive measurement is the key requirement in breast volume measurement, and particularly accurate data acquisition must be completed in a very short time. This requirement

is difficult for the conventional measurement methods to meet.

Three dimensional computer vision techniques have been found to be very effective in the automatic measurement of the living bodies of human beings and animals [27, 74,72]. Information extracted by the vision techniques can guide the process of the measurement automatically and efficiently. The following sections describe active vision techniques employed in determining short-term changes in breast volume by, first, measuring the surface of the breast and then estimating the volume from the surface data.

2.2 A Moiré Topography Approach

Authur *et al.* [7] have developed a Moiré topography approach to measure changes in the volume of the breast between infant feeds. A tungsten-halogen light source obliquely illuminates the breast through a moving Moiré grid to generate contour shadows on the surface of the breast. Photographs of the Moiré topographs are then analysed to produce three dimensional coordinates of transverse sections through the breast. The volume is calculated by multipling the cross-sectional areas by their vertical separation.

2.2.1 The Definition of Breast Volume

It is impossible to measure the absolute breast volume since the separation between chest wall and breast tissue cannot be defined. In the biochemical study, we are concerned with the breast volume changes during the interval between breast feeds rather than the absolute volume. Thus, by including a consistent amount of chest wall in each measurement, changes in volume can be measured accurately. An arbitrary region is defined as the breast volume by enclosing the breast tissue and part of the chest wall. The boundary of this region is drawn on the skin using black non-toxic face paint.

2.2.2 Positioning

The mothers position themselves behind a positioning frame at the beginning of each measurement as described by Authur *et al.* [7]. A general pose taken by the mother is that her arm is raised and rested on an arm rest fixed in the positioning frame over her head and the whole breast is positioned behind the moving Moiré screen and in the common field of view of both the camera and the light source. In order to obtain a reliable estimation of the mean breast volume in a set of measurements, a consistent pose must be adopted during each section of the set of measurements. Repositioning is assisted by using markers fixed on the positioning frame to be matched by marks drawn on the skin.

2.2.3 Summary

A high correlation ($r = 0.97$) is obtained between the change in breast volume before and after feeds as measured by the Moiré topography method and the amount of milk removed as measured by test weighing [7]. Maternal weight change is corrected for evaporative water loss [6] and a milk density of 1.03 g/ml [18] is used to convert milk exchange from weight to volume. The rate of increase in the breast volume between feeds is obtained by linear regression analysis of the interfeed breast volume measurement and this rate is taken as the rate of milk synthesis. A range of 13 to 40 ml/h is obtained for two lactating mothers [7]. The precision of the Moiré topography method depends on the subject repositioning accurately. With careful control over the mother's posture and position, the relative standard deviation between replicate volume measurements is 1.8%, but it is found that inconsistent repositioning can contribute over 10% variation to the replicate volume measurements [7].

Compared with the conventional methods of measuring breast volume, the Moiré topography method is superior to the water displacement method [39] in terms of speed and accuracy [7]. Furthermore, the method is non-invasive which is very important in human body measurements. However, the method involves develop-

ing photographed images and calculating the breast volume manually. The entire process of data processing is therefore laborious and time-inefficient. Besides, the method is limited to restricted breast sizes. Only small to moderate sized breasts are considered, since large sized breasts would have occluded regions which can result in inaccuracy of the measured volume. Investigations of the techniques which measure breast volume automatically and have no restrictions to breast sizes are needed to achieve high efficiency and accuracy.

2.3 A Structured Light System

Based on the SHAPE system as described in Appendix A, the Computerized Breast Measurement (CBM) system has been developed to measure breast volume [38]. The system consists of a 386 IBM PC compatible computer with a Matrox frame grabber, a CCD camera with a zoom lens, a projector that is capable of projecting horizontal light stripes onto the breast surface, and a positioning frame to assist the mother to reposition herself accurately. The projector and the camera are mounted on a stand with the projector placed parallel to the horizon and the camera, which is fixed above the projector, viewing down the object at an angle of 15°. The SHAPE system generates a sample of data points on the breast surface which are submitted to breast boundary detection, data smoothing and pruning if required and volume calculation.

2.3.1 Breast Boundary Detection

A circle encompassing all the breast tissue is drawn around the breast with black face paint. The mother positions herself behind the positioning frame. An intensity image of the breast with the black circle and range data of the breast surface generated by the SHAPE system is submitted to the circle detection and segmentation program [38] where range data outside the black circle are excluded.

2.3.2 Data Smoothing and Pruning

Although the image acquisition time is only around 0.5 second, object movement can still occur during image acquisition and thus erroneous data points can be generated by the SHAPE system. Such invalid data points can be spike points or isolated data points occurring on the very first and/or the very last stripes. The CBM system uses a simple smoothing and pruning process [38,37] to eliminate these erroneous data points.

2.3.3 Volume Calculation

As the breast surface is not the surface of a closed object, its volume is estimated by the volume of the space enclosed by the 3D data points on the breast surface and a reference surface behind the breast. The reference surface is defined by a set of baselines each of which connects the end points of each stripe. As the projector is arranged to be parallel to the horizon, the light stripes from the projector horizontally intersect with the surface of the breast and thus the points on each light stripe form a cross section of the breast.

Volume is calculated as follows [65]: for each stripe, the 3D points on the stripe are projected onto its baseline, and the projection distances (heights) are used to calculate total volume. The volume is then obtained by grouping adjacent points into threes to form triangular prismatic volume elements and summing the volumes of all volume elements. Simple trapezoidal rules are applied in the volume estimation.

2.3.4 Summary

Similar to the Moiré topography approach, the accuracy of the CBM system is established by comparing the change in breast volume before and after breast feeding with the amount of milk removed by the infant as determined by test weighing. The coefficient of variation of replicate measurement is 1.6% [22]. The correlation of the system with test weighing is 0.93 and the rates of milk synthesis between

breast feeds are determined by measuring breast volume at 20 to 30 minutes between breast feeds. A range of 11 to 58 ml/h is obtained for six lactating mothers [22].

Unlike the Moiré topography approach, the CBM system gives an improvement on both the speed and range of breast sizes. The system measures the breast volume automatically. Image capture time is around 0.5 seconds, with an average of 3 minutes for a set of 10 measurements. Breast volume can be estimated within a few minutes in comparison with a few days for the Moiré topography approach. The system also extends the range of breast sizes. Occlusion regions on the surface of large sized breasts are handled by the surface fitting technique [37].

2.4 The Occlusion Problem

All single-view active binocular vision systems have the problem of dealing with missing data at occluded regions which both or either of the sensing devices cannot sense. A similar problem is encountered in breast volume measurement. With the arm raised, the breast tissue lifts up from the chest wall and so the occlusion problem is negligible in general for small breasts. However, occluded regions often occur at the base and lower sides of the breast surface when measuring large or full breasts. Figure 2.1 shows a breast surface with an occluded region at the lower part of the breast surface. Linear interpolation and bivariate quadratic surface fitting [37] have been used in the CBM system in dealing with missing data areas in breast volume estimation.

2.4.1 Linear Interpolation

Missing data areas are simply estimated by straight lines connecting the data points at the boundary of the missing data areas. Each of the lines connects the end points of gaps on the same stripe. Figure 2.2 (a) and (b) display the front view (a) and the side view (b) of the breast after applying the linear interpolation method to the

Figure 2.1: An example of a human breast surface with an occluded region: (a) the front view; (b) the side view.

occluded region in Figure 2.1.

2.4.2 Bivariate Quadratic Surface Fitting

Parametric function fitting techniques are quite common in numerical analysis and computer graphics. The approximating surface using parametric function fitting is expressed in the parametric form

$$\begin{aligned} x &= f_1(s,t) \\ y &= f_2(s,t) \\ z &= f_3(s,t) \end{aligned}$$

where (s,t) are parameters on the surface and f_1, f_2, f_3 are twice differentiable functions to be determined. Given a set of known 3D points on the surface, their coordinates determine a surface that approximates this set of data in the least squares sense and is smooth. Huynh *et al.* [37] have implemented such a technique for solving the occlusion problem in breast volume measurement. The occluded regions are fitted by quadric functions according to the smooth morphology of the breast. Figure 2.2 (c) and (d) display the front view (c) and the side view (d) of

the breast after applying the bivariate quadratic surface fitting technique to the occluded region in Figure 2.1.

2.4.3 Accuracy of Volume Estimation with Occluded Regions

In general, there are four different shapes of female breasts as shown in Figure 2.3 [50,33]. When occluded areas exist on a breast surface, the 3D data points on the surface can not correctly represent the shape of the breast. The approximated surface by the interpolation techniques described above is mainly determined by the distribution of the points at the boundary of the occluded areas. Therefore, small missing data areas may be accurately fitted by the interpolation techniques, but it is difficult to achieve a good approximation of the shapes of large missing data areas. The approximated surface patches to the large missing data regions could give an over-estimation or under-estimation of volume depending on the difference between the real shape of the missing data regions and the fitted surfaces. Figure 2.2 (e) and (f) show the real shape of the occluded region in Figure 2.1 obtained from the other viewpoint. It is noticed that neither the surface patch approximated by the linear interpolation (Figure 2.2 (a) and (b)) nor the surface patch fitted by the bivariate quadratic surface fitting (Figure 2.2 (c) and (d)) accurately match the real shape of the occluded region (Figure 2.2 (e) and (f)). This is because the overall geometry of the breast is unknown and the shape of the occluded region cannot be determined by only the points on the boundary.

The change in breast volume may be measured accurately when the shapes of occluded regions at each measurement are consistent, although a difference may exist between the real volume and the estimated volume by the interpolation techniques. However, it has been noticed that the missing data regions do not have a regular boundary and vary from one measurement to another. In general, there are more missing data areas when the breast is full and less missing data areas when the breast is empty. Since the breast volume is increasing between breast feeds, the

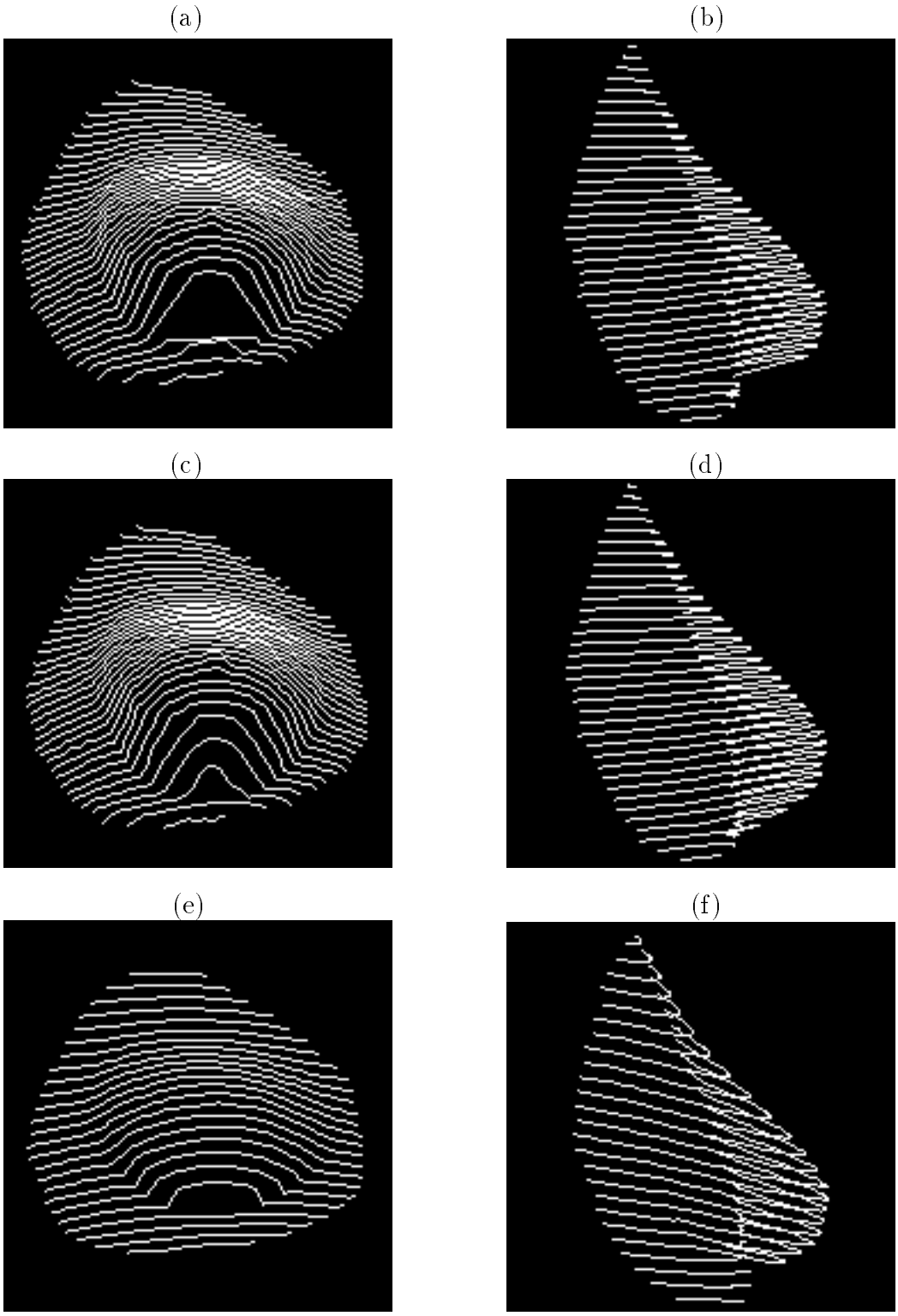

Figure 2.2: A breast surface displayed in front (a) (c) (e) and side view (b) (d) (f) with the approximated surface patch to the occluded region: (a)-(b) by the linear interpolation; (c)-(d) by the bivariate quadratic surface fitting; (e)-(f) the real shape.

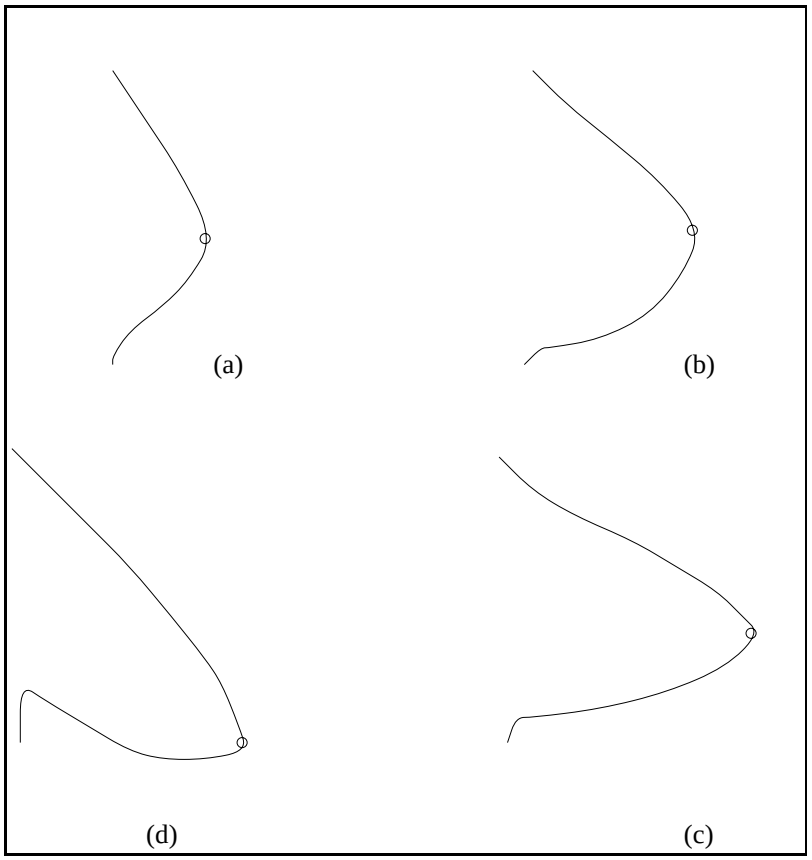

Figure 2.3: Breast shapes:

(a) bowl-shaped:

the anterior projection is smaller than the radius of the circumference;

(b) hemispherical:

the anterior projection is equal to the radius of the circumference;

(c) conical:

the anterior projection is greater than the radius of the circumference;

(d) dependent:

the papillae are pointing downwards.

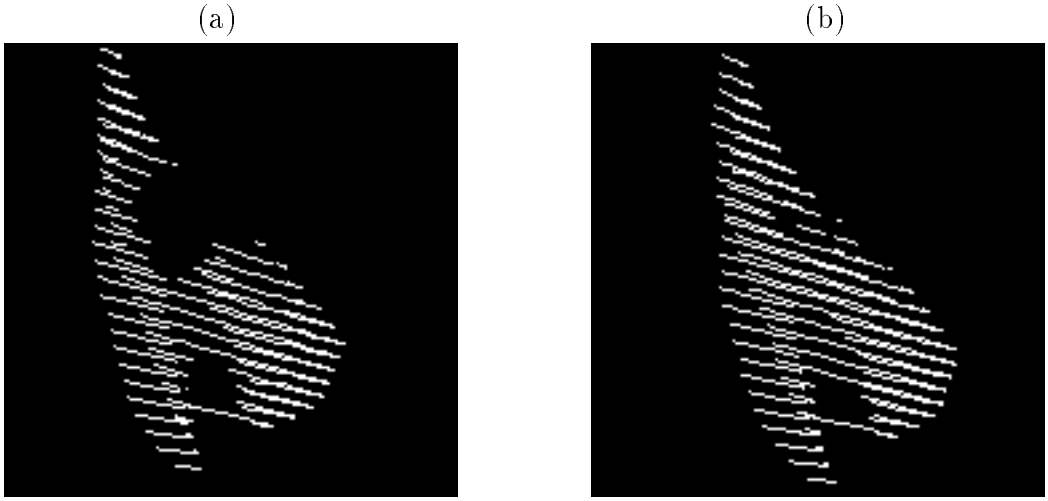

Figure 2.4: An example of a breast surface with different occluded regions before (a) and after feeding (b).

shapes of missing data areas can be different at the different stages of change in breast volume. Thus, the change in shapes of missing data areas is the main factor that contributes inaccuracy in the measurement of short-term changes in breast volume between feeds. Figure 2.4 shows an example of a breast surface with different occluded areas measured before and after feeding. In this example, it is found that the change in breast volume before and after the breast feed is under-estimated by the CBM system compared with the amount of milk removed by the infant as measured by test weighing.

2.5 Conclusion

The computer vision techniques not only provide a fast, non-invasive and accurate measurement tool in determining short-term rates of breast milk synthesis from the changes in breast volume, but also allow the independent determination of the direct influence of the infant's appetite which is important in analysing biochemical factors controlling the synthesis of breast milk.

However, it is found that the measurement of the breast volume from a single viewpoint is not sufficient to infer global 3D surface properties of the breast, thus

inaccurate estimation of the change in breast volume occurs when there are occluded regions on the breast surface. Although the interpolation techniques have been used to approximate the shapes of the occluded regions, the accuracy of the interpolation cannot be guaranteed due to a lack of information on the breast surface. Therefore, more complete information is needed on the breast surface in order to achieve more accurate measurement for all sized breasts. The following chapters describe two methods that perform 3D object measurement from multiple viewpoints.

Chapter 3

Recovering Occluded Regions from Mirror Images

In this chapter, a method is presented for solving the occlusion problem in active binocular vision systems. Combined with a camera and a projector, a mirror is used in the method to create an additional viewpoint to recover the occluded regions which are illuminated by the light source but were previously invisible to the camera. Images from the two views, one directly seen by the camera and the other seen via the mirror, are taken simultaneously.

3.1 Introduction

Most of the techniques for solving the occlusion problem involve creating two or more viewpoints by increasing the number of cameras, projectors, or both at various vantage places. Such multiple-view approaches, whether through moving the object or through moving the sensors, require observing the object over a relatively long period of time to complete the whole measurement, that is, measuring the object from a sequence of viewpoints. Thus, the object must be stationary at all times during the process of capturing images or else errors will occur. However, in certain applications such as the measurement of biological shape, it is difficult to ensure

that the object keep still for more than a couple of seconds. This is especially the case when the measured objects are living bodies of human beings or animals [27,38,74,72]. In order to achieve fast and highly accurate measurement in these applications, a vision system which not only makes measurements from multiple viewpoints but also acquires data at different viewpoints simultaneously is strongly required. We use a mirror, a camera and a projector to design and implement such a vision system. The camera and the projector act as a sensor to obtain 3D coordinates of a sample of points on the object surface by active triangulation, and the mirror provides a virtual viewpoint to recover the regions previously invisible to the camera. An image consists of two parts: one corresponds to the scene directly seen by the camera and the other corresponds to the scene seen via the mirror.

The combination of mirrors with conventional sensors is employed in many applications for the design and implementation of 3D object measurement systems. Mirrors are used as either scanning devices or virtual cameras or both. For example, in active approaches, mirrors are used as simple scanning devices for the scanning of the projection of a light beam [59], and for the synchronous scanning of both the projection and the detection of a laser beam [67]. In biostereometric research, mirrors are used as virtual cameras to create artificial viewpoints for 3D shape measurement of human bodies simultaneously. The NEL range finder [66] uses a mirror as both a scanning device and a virtual camera in such a way that a laser beam is swept across a scene by a rotating mirror and the scene is then viewed in the same mirror by a camera. In other measuring systems [64,53,48], the sensing device is composed of a single pair of photogrammetric cameras and two mirrors. A set of control points or marked anatomical points on the surface of the human body are automatically measured at the same time. The 3D data are obtained by using passive sensing techniques, and simultaneous data acquisition is achieved by using mirrors to solve the problem of unavoidable movement of the living body. The use of conventional stereophotogrammetry and mirrors allows one to measure sparse and marked anatomical data at the same time. In order to obtain dense measurements simultaneously, one may need to combine mirrors with active sensors.

In our system [28], a mirror is combined with an active binocular system that consists of a camera and a projector. The projector projects an array of binary coded light stripes onto the object surface to be measured. The need to scan a light stripe is therefore avoided. We use the mirror as a virtual camera/projector pair to provide more information from a virtual viewpoint. The SHAPE system is employed in our implementation.

3.2 A Virtual Viewpoint via a Mirror

3.2.1 System Geometry

The system arrangement is depicted in Figure 3.1. The mirror is placed near the occluded part of an object with a suitable orientation. A scene, including the normally occluded region, is reflected by the mirror and the mirror image of the scene is then captured by the camera. The camera is displaced from the projector that illuminates the measured object with an array of binary coded horizontal light stripes.

When a mirror is included, a virtual object is created. It is the mirror reflection of the real object. The scene observed by the camera can be divided into two parts: *the real scene* corresponding to the real object, and *the virtual scene* corresponding to the virtual object.

It is important to understand the geometric meaning of the virtual scene. Let us imagine that there is a *virtual camera* behind the mirror. This virtual camera is placed in such a location as if it was the mirror reflection of the real camera. The virtual scene is actually the mirror reflection of what the virtual camera sees of the real object. In fact, the mirror provides a second viewpoint at the location of the virtual camera. Thus, the occluded regions invisible to the real camera become indirectly visible through the mirror. These occluded regions can then be measured using the geometrical properties of mirrors.

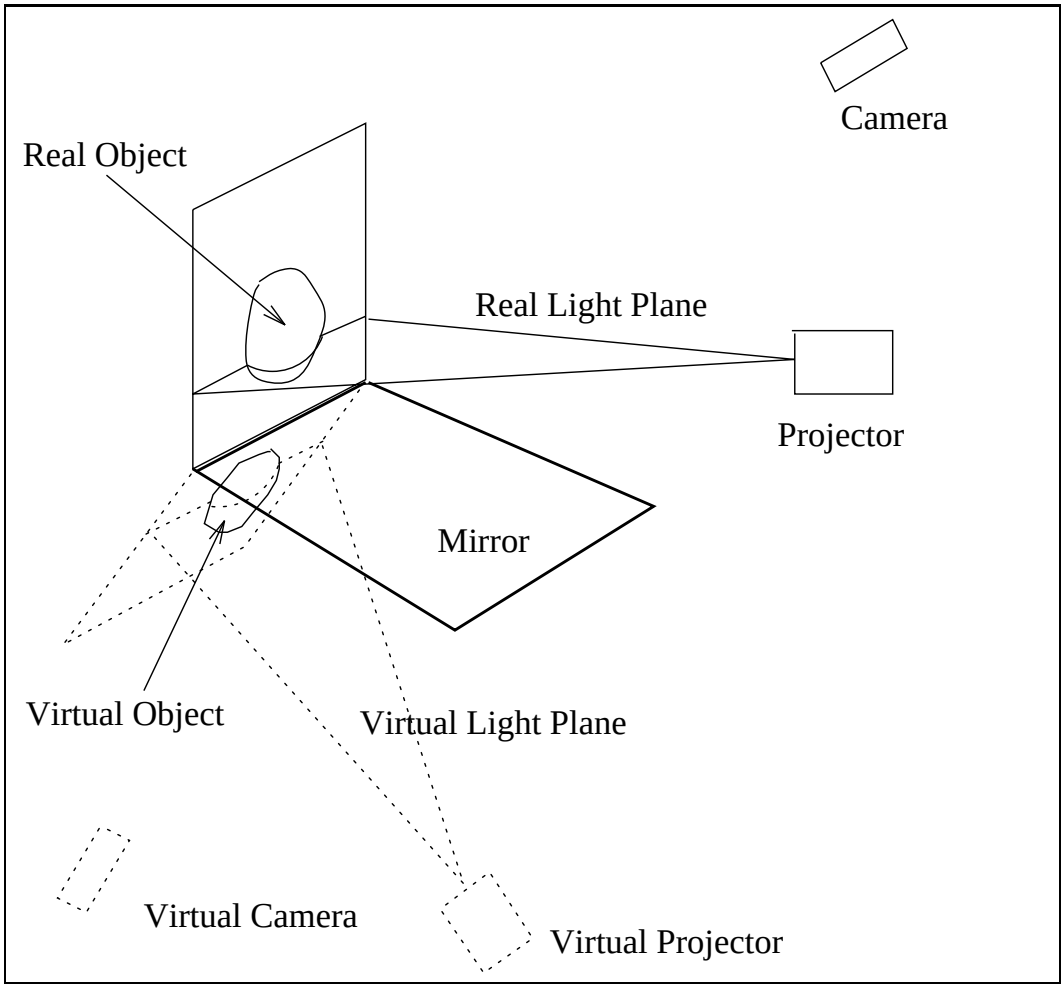

Figure 3.1: Camera, projector and mirror geometry.

Two stages are involved in the reconstruction of the occluded regions. First the virtual object should be reconstructed from the mirror images. The second stage is to convert the points in the virtual object to their corresponding points in the real object.

3.2.2 Virtual Object Measurement

In active structured lighting methods, the 3D coordinates of a point on the measured object surface can be obtained by finding the intersection of the line defined by the 2D image coordinates of that point and the plane defined by the sheet of light forming the stripe [16]. The part of the object directly visible to the camera can be easily measured by triangulation. We concentrate on the measurement of the virtual object - the "object" inside the mirror.

As shown in Figure 3.1, we use the term *real light* to represent the light illuminating the real object, and *virtual light* to represent the mirror reflection of the real light which can be considered as the light illuminating the virtual object from the virtual projector. Each virtual light plane corresponds to a unique real light plane.

The 3D coordinates of the point on the virtual object can be determined by the intersection of the line defined by its 2D mirror image coordinates and the plane defined by the virtual light plane.

As the position of the camera and the projector are all known, the key component in the virtual object measurement is to decide the position of the mirror and thus find the virtual light planes that "illuminate" the virtual object.

A Pencil of Planes

A family of planes that intersect in one common line is called *a pencil of planes*, and is illustrated in Figure 3.2. Given any two planes $\mathbf{n}_1 \cdot \mathbf{x} + p_1 = 0$ and $\mathbf{n}_2 \cdot \mathbf{x} + p_2 = 0$ contained in a pencil of planes, a general equation of the pencil of planes can be

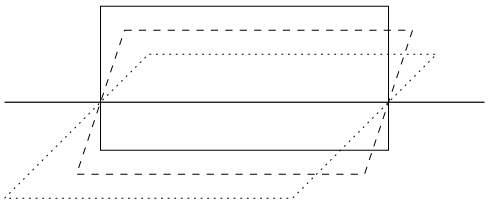

Figure 3.2: A pencil of planes.

represented by the following equation [30]:

$$(\mathbf{n}_1 \cdot \mathbf{x} + p_1) + \lambda(\mathbf{n}_2 \cdot \mathbf{x} + p_2) = 0 \tag{3.1}$$

where $\mathbf{n}_1 \times \mathbf{n}_2 \neq 0$. For each value of λ, the equation represents a plane in the pencil of planes.

In our system, the plane of the mirror, the planes of the real light stripes and the planes of the virtual light stripes consist of a pencil of planes. If the equations of the mirror plane and a plane of a real light stripe are known, the equation of the corresponding virtual light plane can be determined by solving for λ in equation (3.1).

Virtual Light Planes

Given the equation of the mirror plane

$$\mathbf{n}_m \cdot \mathbf{x} + p_m = 0 \tag{3.2}$$

and the equation of a real light plane $\mathbf{n}_r \cdot \mathbf{x} + p_r = 0$, according to equation (3.1), the equation of the virtual light plane corresponding to the real light plane can be represented by $(\mathbf{n}_r \cdot \mathbf{x} + p_r) + \lambda_v(\mathbf{n}_m \cdot \mathbf{x} + p_m) = 0$ which can be rewritten as

$$\mathbf{n}_v \cdot \mathbf{x} + p_v = 0 \tag{3.3}$$

where

$$\mathbf{n}_v = \mathbf{n}_r + \lambda_v \mathbf{n}_m, \tag{3.4}$$

and

$$p_v = p_r + \lambda_v p_m. \tag{3.5}$$

The λ_v can be determined by the relations between the plane of the mirror and the planes of the pair of real and virtual light stripes as shown in Figure 3.3. The figure shows a side view of the geometry such that the planes defined by the mirror, and the pair of the real and virtual light stripes, appear as lines. The $\mathbf{n}_m$, $\mathbf{n}_r$, and $\mathbf{n}_v$ are, respectively, the normal vector of the mirror plane, the real light plane and the virtual light plane. Since each pair of real and virtual light planes is symmetrical about the mirror plane, the angle between the vector $\mathbf{n}_m$ and $\mathbf{n}_r$ is equal to the angle between the vector $-a\mathbf{n}_m$ and $\mathbf{n}_v$. From the diagram we see that

$$\mathbf{n}_v = \mathbf{n}_r - a\mathbf{n}_m. \tag{3.6}$$

Let θ be the angle between the plane of the mirror and the plane of the real light stripe. We have $\cos(\theta) = \mathbf{n}_m \cdot \mathbf{n}_r$ and $\cos(\pi - \theta) = \mathbf{n}_m \cdot \mathbf{n}_v$, thus $\mathbf{n}_m \cdot \mathbf{n}_r = -\mathbf{n}_m \cdot \mathbf{n}_v = -\mathbf{n}_m \cdot (\mathbf{n}_r - a\mathbf{n}_m)$ and $a = 2(\mathbf{n}_m \cdot \mathbf{n}_r)$. Therefore, the λ_v in equation (3.4) and (3.5) is determined by $\lambda_v = -a = -2(\mathbf{n}_m \cdot \mathbf{n}_r)$ from equation (3.6).

3.2.3 From Virtual Object to Real Object

A point in the virtual object can be easily transformed to its corresponding point in the real object. Given the equation of the mirror plane, from the symmetrical property of mirrors, the virtual point lies on the line drawn from the real point perpendicular to the mirror and is as far behind the mirror as the real point is in front of it. Thus given a virtual point $\mathbf{x}'$ on the virtual object, the corresponding real point $\mathbf{x}$ can be obtained as follows:

$$\mathbf{x} = \mathbf{x}' - 2d\mathbf{n}_m \tag{3.7}$$

where $d = \mathbf{n}_m \cdot \mathbf{x}' + p_m$ is the oriented distance from $\mathbf{x}'$ to the mirror.

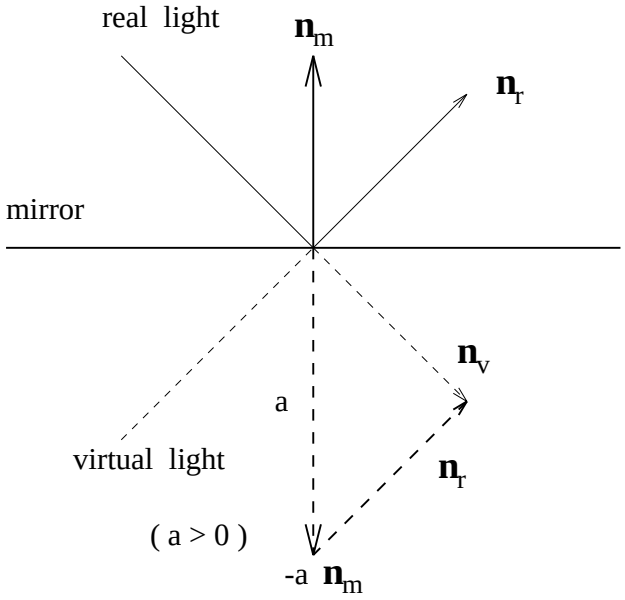

Figure 3.3: Relations between the plane of a mirror and the planes of a pair of real and virtual light.

3.3 Implementation

An image obtained by the camera consists of two parts: the real image corresponding to the real object and the mirror image corresponding to the area seen via the mirror. Any conventional active binocular vision system consisting of a projector and a camera can be used to extract the 3D information contained in the real image, but it could not correctly calculate the 3D information of the measured object contained in the mirror image without account of the existence of the mirror being taken. The following sections give the details of the implementation of recovering 3D information of the surface from the mirror images using the SHAPE system described in Appendix A.

3.3.1 Mirror Calibration

Besides the calibration of the camera and the projector required by the SHAPE system, mirror calibration is needed in our system. The calibration of the mirror finds the equation of the mirror plane (3.2), which is achieved by measuring some sample points of the surface of the mirror using the SHAPE system. The position of the mirror is determined by fitting a plane to these sample points using the least squares fitting technique. Due to mirror reflection, thin tape is used to mark the positions of the sample points on the mirror. In practice, 12 sample points are used.

3.3.2 Reconstruction from Mirror Images

After finishing the calibration of the camera, the projector and the mirror, eight images of different stripe patterns are taken by the camera. These images are then segmented into 8 real images and 8 mirror images. The SHAPE system is used to measure the 3D coordinates of the points on the real object by taking the 8 real images as its input directly. The 3D coordinates of the points corresponding to the surface area seen through the mirror are recovered in the following steps.

- First, equation (3.3) is determined for each of the virtual light planes corresponding to each stripe as seen in the mirror image.
- These light planes are then fed to the SHAPE system together with 8 mirror images to obtain the 3D coordinates of the points on the surface of the virtual object – the "object" inside the mirror.
- These points are then converted to the corresponding points on the surface of the real object by equation (3.7).

Finally the completed surface of the object is formed by merging the two surface patches. For the same point to be visible to both the camera and the mirror, it is noticed that there is always a difference in the range caused by calibration errors. The range directly determined by the real images should be more accurate than

the range recovered from the mirror images as no mirror is involved. Therefore, the point directly seen by the camera is kept and the point recovered from the mirror images is discarded.

3.4 Experimental Results

We have conducted a number of experiments using the system on a coffee mug and two breast models with different occluded areas. Experiments have also been done on the measurement of human breasts. These experiments are performed by positioning the mirror near the lower part of the measured object to make the occluded region in this part visible to the camera via the mirror.

Figure 3.5 and Figure 3.6 show the experimental results from one of the breast models in which 214 points are recovered from the mirror. The average difference in 3D distance between the overlapped points which are seen by the camera both directly and indirectly via the mirror is 5 mm. Similar results are obtained for the experiments on human breast measurement. Figure 3.7 and Figure 3.8 show the experimental results with the coffee mug in which 147 points are recovered from the mirror. The average difference in 3D distance between the overlapped points is 1.5 mm. The results compared favourably with those obtained without using the mirror.

3.5 Discussion

The accuracy of shape measurement via mirrors is mainly determined by sensor calibrations. The details of error analysis of the SHAPE system can be found in [3]. The local defects of the mirror surface may result in inaccurate measurement in two cases. One is unsharpness of the local image if variations occur within a tiny surface which can affect the accuracy of stripe location. The other is local parallax, either transverse or longitudinal or both simultaneously, which can lead to a loss

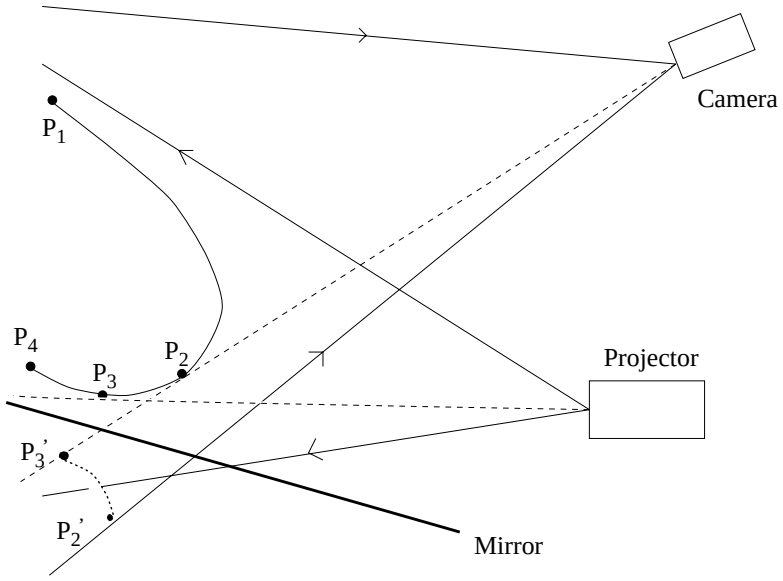

Figure 3.4: The field of view of a camera and a projector with a mirror.

in local model consistency (observable transverse parallax) and to resulting errors along any coordinate axis [48].

The advantages of combining a mirror with active approaches can be seen from Figure 3.4 which shows the field of view of a camera and a projector in which P_2 is the last point on the section boundary facing the camera and P_3 is the last point on the boundary illuminated by the projector. The common area visible to both the camera and the projector is the segment P_1P_2. The segment P_2P_3 is an occluded area invisible to the camera but illuminated by the projector. Firstly, with the use of a mirror, the segment P_2P_3 can be recovered from its mirror reflection segment $P_2'P_3'$. Furthermore, it is known that all projecting methods have to make a tradeoff between measurement accuracy and data deficiencies. Increase of accuracy and decrease of data deficiencies are mutually exclusive. The mirror can be used to solve this problem. With the mirror included in our system, the angle between the camera and the projector can be extended to achieve high accuracy while the occluded areas are not increased if the areas resulting from the larger separation of the camera and the projector can be recovered from the mirror images. Finally, the use of a mirror also provides a simple means for simultaneous data acquisition

which is very important in biological shape measurement.

A limitation of our system is that it does not use the mirror as a scanning device so that the interference between the light from the projector and the light reflected by the mirror should be avoided. One of the disadvantages of our system is that it can only recover areas invisible to the camera, but visible to the projector. The segment P_3P_4 is unmeasurable in our system, for the segment is neither visible to the camera nor to the projector. The other disadvantage is that there is no flexibility to select the position of the virtual viewpoint in accordance with the complexity of the object surface, since the positions of the virtual camera and the virtual projector are restricted by the positions of the real camera and the projector. However, this can be achieved by using multiple sensors. Chapter 4 will discuss such an approach using two pairs of a camera and a projector.

The 2D feature detection is crucial to 3D shape measurement. It has been noticed that the quality of the stripes projected onto the occluded regions is an important factor in our method. The quality of stripes is determined by their density, brightness and sharpness. Stripes with poor quality may be recognised by human beings but it is difficult for vision techniques to extract such features. It is found that some poor quality stripes in the occluded region cannot be located by the SHAPE software so that the occluded region cannot be recovered, although it is seen by the camera via the mirror. An example of this situation is shown in Figure 3.6 (c) where the stripes at the lower and side parts of the model cannot be located due to their poor quality. The same situations are also encountered in human breast measurement. More powerful techniques for edge detection or 2D feature detection such as using deformable models [43] may be needed in the future to detect stripes with poor quality.

3.6 Conclusion

A short phase of instantaneous image acquisition is often a constraint imposed by many computer vision applications, particularly in the application to the measure-

ment of biological shape such as measuring human bodies. A simple method of combining a mirror with an active approach is presented in this Chapter. This method can be used to solve the occlusion problem in active binocular approaches in the occluded region that is illuminated by the projector but is invisible to the camera. Compared with other multiple view approaches, this method is not only simple and low cost but more importantly it performs measurement on multiple views simultaneously.

(a)

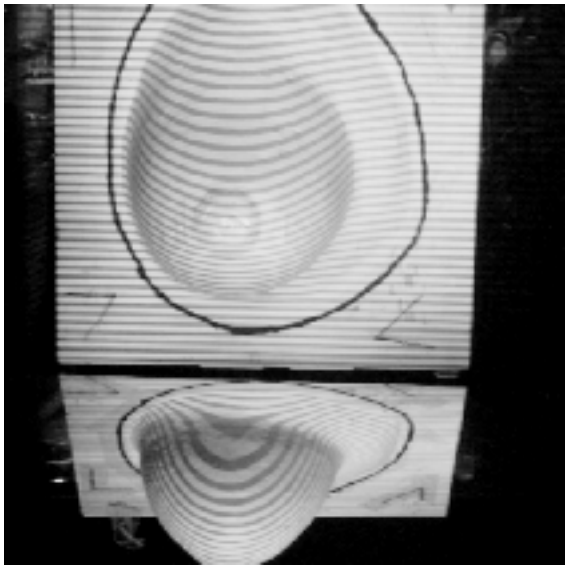

(b)

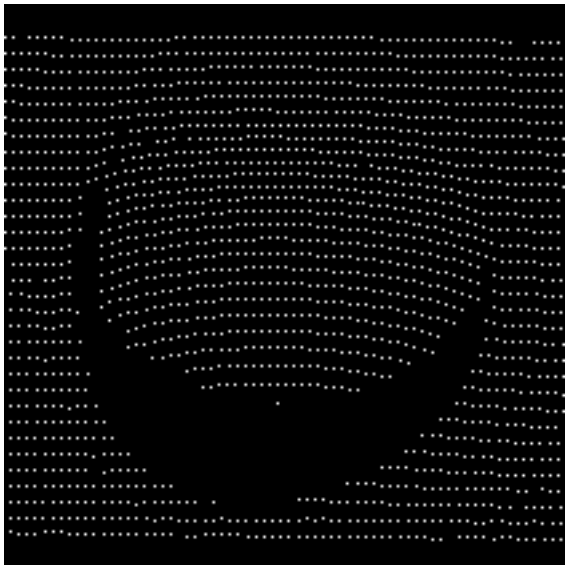

Figure 3.5: A breast model: (a) the grey level image showing both real scene and virtual scene; (b) the measurement of the real object, rotated by 10°.

(c)

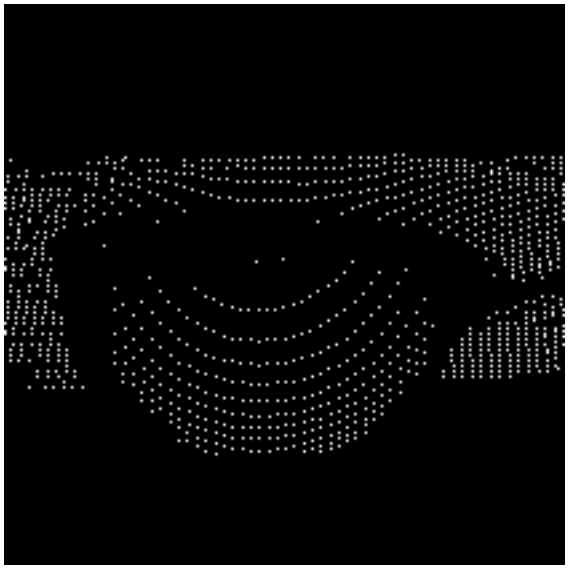

(d)

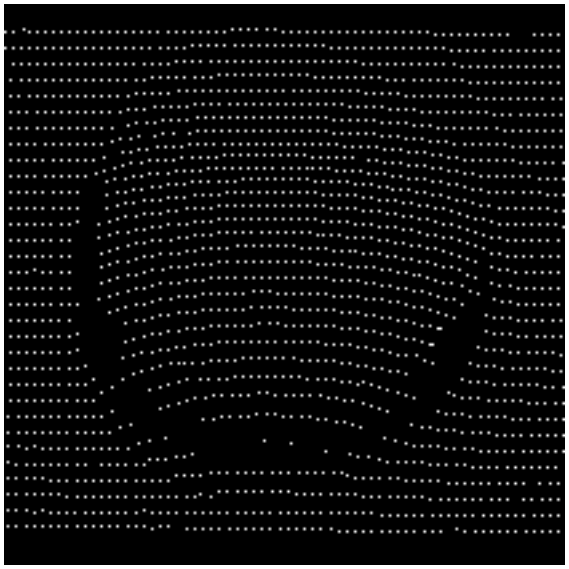

Figure 3.6: A breast model: (c) the measurement of the virtual object; (d) the result by merging (c) and Figure 3.5 (b), rotated by 10°.

(a)

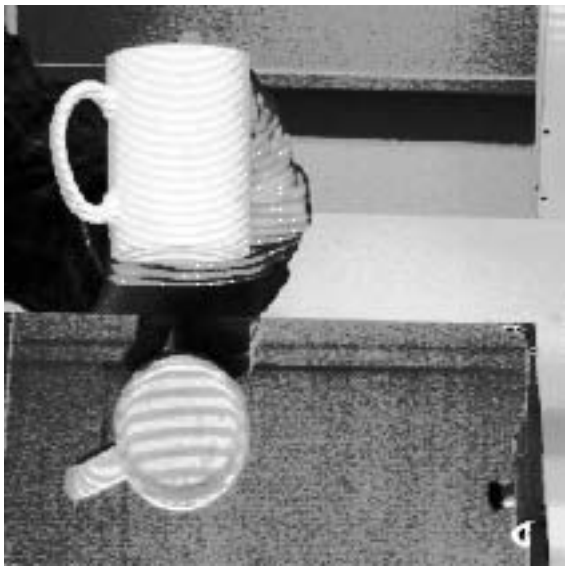

(b)

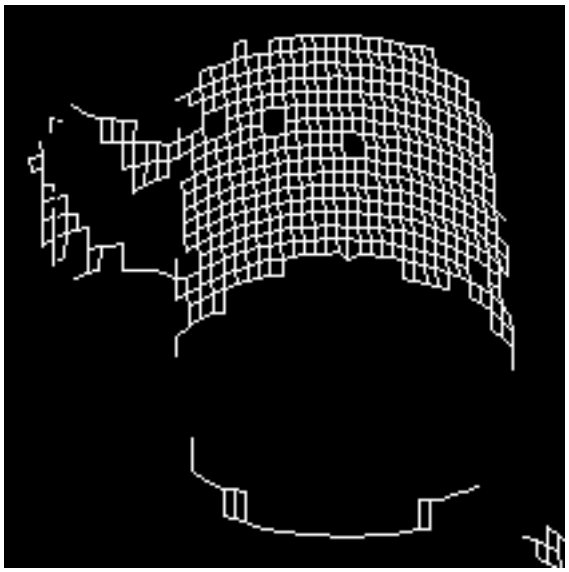

Figure 3.7: A coffee mug: (a) the grey level image showing both real scene and virtual scene; (b) the measurement of the real object, rotated by 30°.

(c)

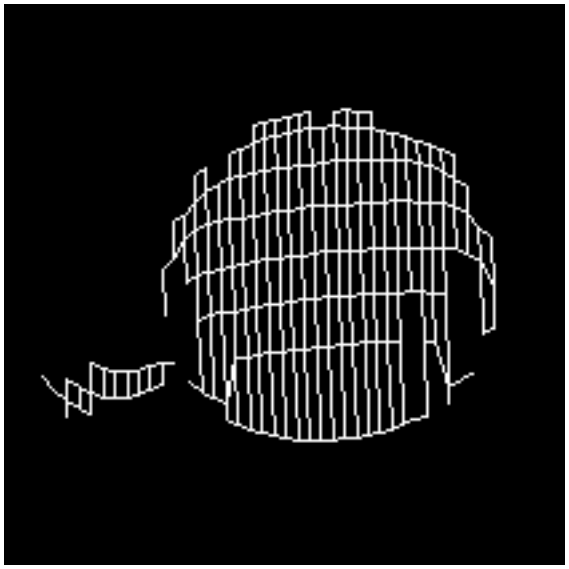

(d)

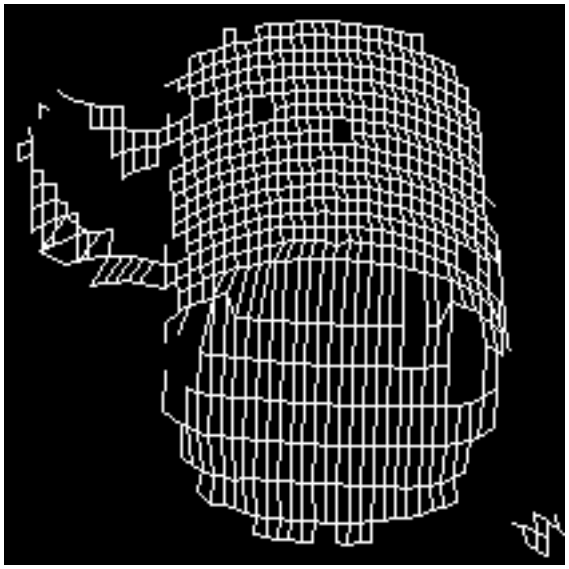

Figure 3.8: A coffee mug: (c) the measurement of the virtual object; (d) the result by merging (c) and Figure 3.7 (b), rotated by 30°.

Chapter 4

3D Shape Measurement from Multiple Views

The complete 3D description of the surface of objects requires the acquisition of several images from different vantage viewpoints. Each image contains information on the part of the object that is visible from its viewpoint. A very important task consists in the integration of the information present in each view. This chapter discusses various approaches of 3D model construction from multiple views and presents an implementation of such a system developed for of the biochemical study of breast surface and volume measurement in women.

4.1 Introduction

All the ranging techniques based on a single view face the problem of viewing constraints, *i.e.*, the 3D data provided conveys information only for the "visible" part of the scene. The description of the object of interest is often affected by occlusion problems. Observing an object from multiple viewpoints is required for a more complete description of the surface of the object. Several images must be acquired from different viewpoints and view integration must be performed. The extra information available from additional views is entirely due to the geometrical

constraints that arise from the motion of the sensors or the object.

Several methods have been developed in the past to create a multiple-view sensor by (1) maneuvering the sensor(s) around the scene at different vantage viewpoints [61]; (2) rotating and translating the scene (objects) in front of the sensor(s) [12, 75,14,68]; (3) using multiple stationary sensors in different locations to capture the appropriate views [24,74], or (4) any combination of these methods [42]. The process of creating a multiple view ranging system involves solving the following problems: data acquisition at each view, registration between views, and integration of views for surface reconstruction. The aim of data registration is to find a rigid spatial transformation from one view to the other so that all data from different views can be transformed to a common coordinate system. The surface segments of all views consist of the overall surface of the object with overlapped portions between adjacent views. The integration of views combines registrated surface segments into a completed surface representation.

Surface matching is one of the methods for finding view registration. Potmesil [61] generates models for 3D objects by spatially matching 3D surface segments obtained from a large number of views. A depth map at each view is generated using a white-light, grid-projecting, triangular-based range finder. Range data for object surfaces are fitted with a sheet of parametric bicubic surface patches which are then recursively merged into a quadtree hierarchical structure. Surface matching is defined as "finding a spatial registration of two surface descriptions that maximizes their shape similarities". His matching algorithm uses an heuristic search to align overlapping surface segments into a common 3D coordinate system. Once a surface segment match is determined, a merging algorithm generates a new surface for each matched surface segment. A complete object model is created by sequentially interleaving the matching and merging processes. Ferrie and Levine [26] describe an approach to multiple view integration based on matching surface features to obtain interframe correspondence. The accuracy of this approach depends on the accuracy of the feature detection technique used. Chen and Medioni [19] develop an algorithm for surface registration by assuming that the surfaces are approximately

registered. The registration algorithm is an iterative process minimizing a least square error measure between the distance from points to planes. These correspondence based methods are quite useful in general, particularly when the movement of sensors or objects is difficult to determine by other techniques, and they also provide flexible means for creating a complete 3D model without constraints on the path of the movement of sensors or objects. However, these methods are computationally expensive due to the large search space that needs to be explored for establishing correspondence.

Research has also been devoted to 3D object modelling by assuming that the inter-frame transformation is known a priori. Bhaun [12] develops an object modelling system for object recognition by rotating an object through known angles to acquire multiple views, and the surface of the object is then represented by planar faces. Chien *et al.* [21] and Ahuja and Veenstra [2] generate octree object models using orthographic views. Saint-Marc *et al.* [68] describe a range finding system using a linear or rotary table to obtain complete object description. With a priori knowledge of objects or sensor movement, the transformation between views is easily established once the sensors are calibrated. These techniques are simple and fast in the registration of views but may limit the movement of the object relative to the sensors, or the sensors can only be at certain locations. In addition, they may require an expensive precision positioning device to keep track of the translations and rotations of the object or sensors.

The use of image geometry has been investigated in some of the multiple view vision techniques. Vemuri and Aggarwal [75] present a technique using image geometry to determine the surface registration by observing the orientations of a base plane pattern in the intensity images of multiple views. The base plane is encoded with a pattern consisting of a single straight line. The object is positioned on the base plane such that the base plane pattern is fully or partially visible from every viewing angle. The merged data is expressed in a cylindrical coordinate system. Boey [14] describes a 3D modelling method by spacing control marks around the object. The object is positioned such that the control marks are fully visible to each viewpoint. The 3D

coordinates of these control marks are determined by using stereo disparity. The interframe transformation can then be deduced by point-to-point correspondence established between the control marks in adjacent views. Data merging is achieved by resampling techniques. These techniques depict an effective way to integrate information from both range and intensity images.

One of the practical approaches to 3D shape measurement from multiple views is based on using multiple stationary sensors to achieve complete 3D modelling. Instead of moving the object or the sensors, stationary sensors are spaced around the object at different viewpoints to obtain a partial surface measurement at each viewpoint. The sensors can be arranged at known locations such that interframe transformations between views is easily established. In addition, the shape measurement systems at all viewpoints can be calibrated with respect to a common coordinate system. Thus, partial surfaces obtained from these viewpoints can be integrated without the additional step of finding interframe transformations. Dimatteo *et al.* [24] hold a patent for the arrangement of sensing the geometric characteristics of an object. Four camera/projector systems are positioned in spaced relationships about an object for the purpose of covering the entire surface of the object. The projectors are operated cooperatively with all projectors having identical projected patterns. The drawback of the arrangement is that the bottom surface cannot be measured without an extra sensor positioned below the object in space. Vannier *et al.* [74] develop a noncontact 3D digitizing system for the measurement of the surface of the human head. The system employs a stationary, multiple-sensor fixed scheme to meet the requirements of 3D surface coverage, accuracy, speed and automatic processing in the specific application of facial plastic surgery. They space three sensors circumferentially around and slightly above the subject, with three more interleaved among them but slightly below the subject's head. These six sensors thus form a zig-zag pattern around the subject's head providing coverage of areas that a single sensor restricted to a motion path could not easily sense. At each viewpoint, the sensor consists of a camera and a projector. 3D data is generated by triangulation using structured lighting. The process of measuring surface patches is carried out for all camera/projector pairs to form six surface patches in sequence.

The system then combines the surface patches using 3D transformation and 3D resampling to form a complete surface representation of the scanned subject. Jones *et al.* [42] describe a scanner for the measurement of a human body size and surface shape for applications in the textile manufacturing industry. The system combines the approaches based on moving the object with the approaches based on multiple stationary sensors. Sixteen projectors and fourteen cameras are positioned around the subject who stands on a turntable. The whole surface of the human body is measured by rotating the table through 360 degrees in measured increments. The approaches based on using stationary sensors at different viewpoints can be applied to real time applications as they can avoid the disadvantages caused by shifting or rotating the object or the sensors, which could result in inaccuracy during movements. However, such approaches may need the use of numerous sensors in order to cover the surface of the object of interest which might be cost effective compared with approaches based on moving sensor(s) or the object.

No single method is suitable for all applications. In some cases, sparse 3D data are all that is needed to understand a scene, while in others, dense 3D data are required to represent the 3D structure of an object. Industrial processes often impose tight constraints on range-image acquisition time, and medical applications also require highly accurate measurement. Therefore the choice must be made between static or dynamic rangefinding techniques depending on the requirements of the application.

In our application, fast, accurate, non-contact measurement is the key requirement in the breast surface and volume measurement. It has been shown that the breast volume changes according to whether the lungs are inflated or deflated. Hence accurate data acquisition must be completed in a very short time as discussed in Chapter 2. We have developed a two view system [29] based on stationary sensors (camera/projector pairs) to meet the requirements of this application, particularly, to solve the occlusion problems in the single view system [37,38].

As described in Chapter 3, the occlusion problems may be solved by the method of combining a mirror with active vision methods. However, the method can only be used to recover the occluded regions invisible to the camera, thus having limited

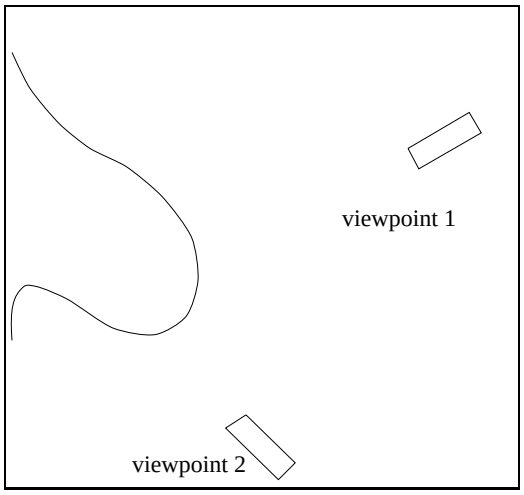

Figure 4.1: Geometry of two camera and projector pairs.

use for the occluded regions visible to neither the camera nor the projector. Such occluded regions are often encountered in measuring large sized breasts. Therefore, the development of techniques for 3D shape measurement using multiple sensors is needed.

We employ the method of multiple stationary sensors rather than a moving-sensor or the moving-object approach for several reasons. First, with no mechanical motion required of either the sensors or the object, the speed requirement is achieved in data acquisition and inaccuracy caused by object movement can be reduced. Second, by spacing each sensor at a vantage point, we have positioning flexibility in order to reach portions of the surface perhaps not viewable by other methods, such as a single sensor moving about the object, or the object moving about the sensor on a fixed path. Finally, we can select the number of sensors based on the object surface's complexity so that the system can be applied to different sized objects.

4.2 System Arrangement

In the two view system, a sensor at each viewpoint consists of a projector and a camera. Two sensors are placed at vantage points around the object acquiring range

data sequentially. The system arrangement are illustrated in Figure 4.1. The first viewpoint is in front of the object and the second is below the first one. The system setup can largely eliminate the occlusion regions at the lower part of the object and provide coverage of most areas of the object surface. At each viewpoint the SHAPE system is used to obtain range data represented by a sample of 3D points. All data from different views are integrated into an object-centered coordinate system and resampled by a single parametric grid using piecewise linear interpolation.

4.3 Calibration and Triangulation

Camera and projector calibration is the process of determining the internal camera and projector geometric and optical characteristics (intrinsic parameters) and the 3D position and orientation of the camera and projector frame relative to a given world coordinate system (extrinsic parameters). The DLT (Direct Linear Translations) method [16,73] is used for both camera and projector calibration in the SHAPE system. In the DLT method the camera is modelled by a transformation matrix which maps 3D world coordinates of a point into the 2D image coordinates, and the projector is modelled by a plane equation which relates the world coordinates of a point to the y image coordinate (stripe code) of the stripe on which the point lies. The details of the calibration technique have been discussed in Section A.2.3. In the two view system, the two camera/projector pairs are calibrated in a global coordinate system using the calibration technique provided by the SHAPE system.

3D coordinates of a sample point are determined by triangulation which involves finding the intersection of the line specified by the camera's image coordinates on a stripe center and the plane defined by the stripe code. A visible portion of the object surface at each view is presented by an array of sample points sorted according to two parameters u and v, where u is the first dimension of the array indexed by the order of stripe numbers and v is the second dimension indexed by the order of column numbers along each stripe. A breast model is used in our experiments.

Figure 4.2 and 4.3 show the intensity image (a) and the 3D wireframe model (b) of the breast model viewed from, respectively, the first viewpoint and the second viewpoint. As shown in the figures, a single view is not sufficient to measure all the surface of the model.

4.4 Surface Resampling

Using active structured lighting techniques, the surface sampling is determined by the pattern and orientation of the structured light used. Depth information can be extracted only on the portions of the surface with light illumination. Various forms of structured light can be used, such as rays, sheets or grids. Most single view systems employ structured light with a regular pattern, such as a set of horizontal light strips employed by the SHAPE system. Thus a regular surface sample may be formed by a set of sample points on the surface using the single view systems. However, in multiple view systems the surface sample of an object may become irregular for two reasons. First, different light patterns may be used at different viewpoints, giving irregular overall sample data. Second, even though the same light pattern is used at all viewpoints, irregularity still occurs in the combined sample data due to the different orientation of the light sources. Figure 4.4 illustrates a combined surface sample from two adjacent viewpoints. A surface sample of the breast model with an irregular pattern is shown in Figure 4.5 which is obtained by simply combining the two partial surfaces observed from the two viewpoints.

A well-defined representation of 3D shape of the human body surface is often required for the clinical problems such as calculating the area of a patch of surface, estimating the volume enclosed by a portion of surface, and determining the most likely correspondence between two surfaces. As shown in Figure 4.5, the combined surface sample does not provide a well-defined representation of the surface. A process of surface reconstruction is therefore needed to integrate 3D data from multiple views.

There are at least three important functions served by surface reconstruction. First,

(a)

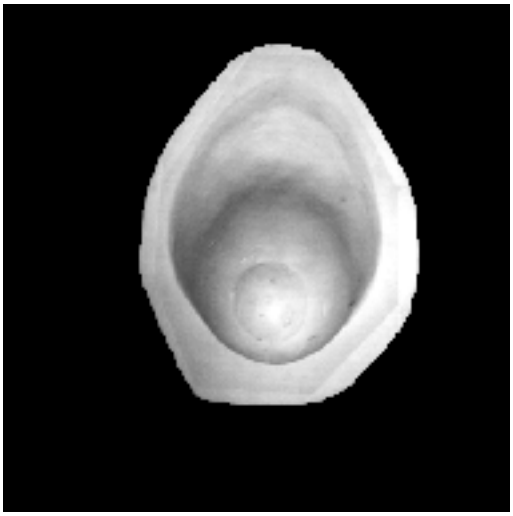

(b)

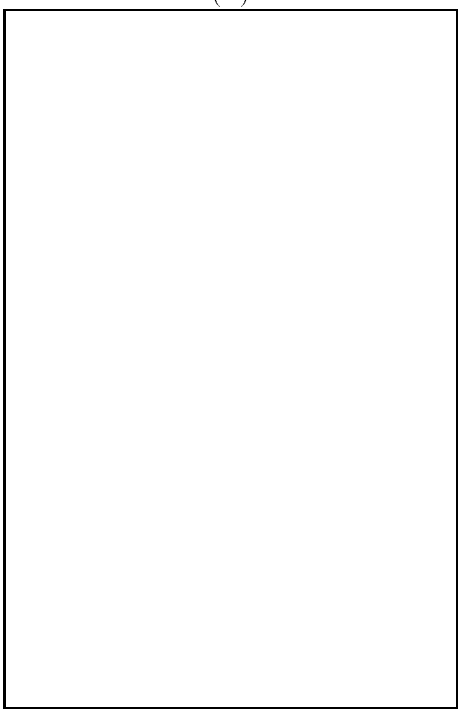

Figure 4.2: A display of a breast model at the first viewpoint: (a) the intensity image; (b) the 3D sample data.

(a)

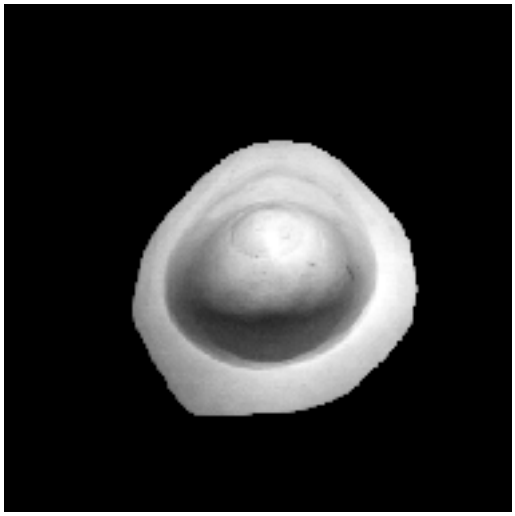

(b)

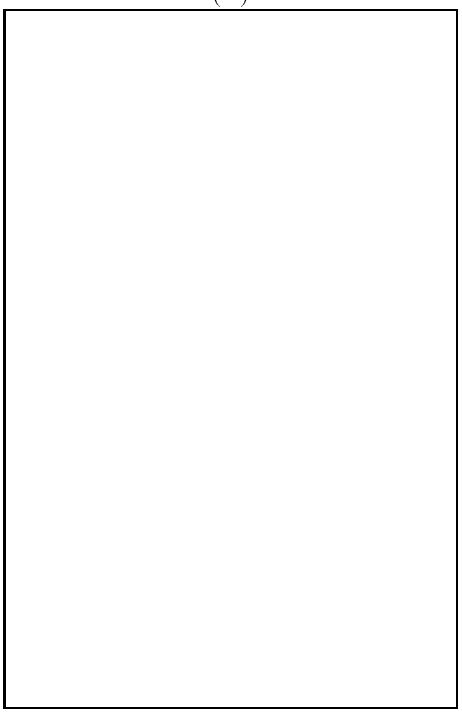

Figure 4.3: A display of a breast model at the second viewpoint: (a) the intensity image; (b) the 3D sample data.

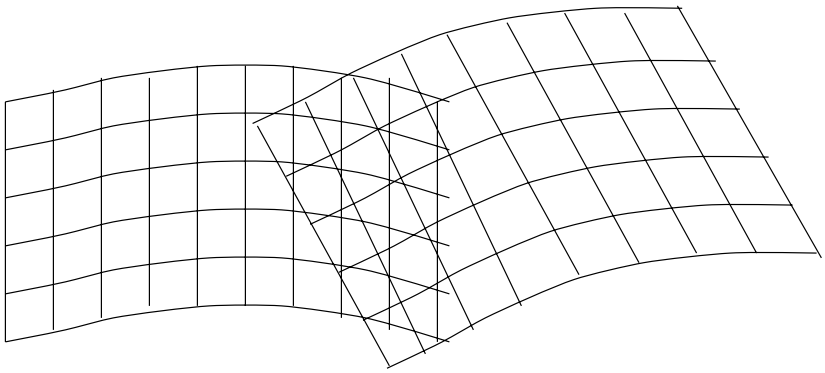

Figure 4.4: Surface segments.

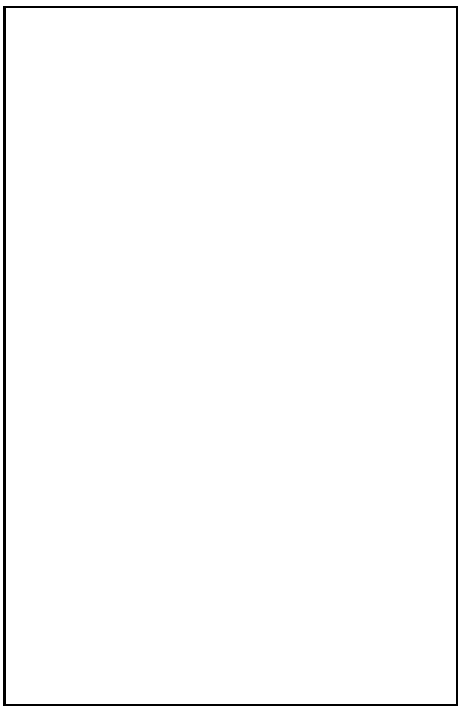

Figure 4.5: Combined data from the first and the second viewpoint.

surface reconstruction interpolates gaps in the original data. Second, surface reconstruction combines information about surface shape from various sources. Third, surface reconstruction smooths the observed data. The methods for surface reconstruction can be generally classified as surface-based approaches or volume-based approaches [9,15]. Surface-based approaches have been reported in the literature [61,12,75,74] in which the surface of the object can be described by a single closed parametric grid. Volume-based approaches [45,58,21] to the problem describe the object volumetrically and do not provide direct surface information about the object.

Cylindrical and spherical coordinate systems centered in the object are commonly used in surface-based approaches for resampling the surface of curved objects. These two coordinate systems are selected based on the shape of the object, e.g. for an elongated shape cylindrical coordinates may be used, and for a spherical shape spherical coordinates may be used. An object-centered reference frame is one which depends on the structure and the shape of the object rather than the observer's projected view. The use of an object-centered reference frame can thus avoid problems with variable density of surface sample, *i.e.*, some of the surface areas are closely sampled but some of the surface areas are coarsely sampled [14,19]. Once the object-centered coordinate frame has been selected, 3D data from each view of the object is transformed to this coordinate frame. These data are then further reparameterised through interpolation into a uniform array of cylindrical or spherical coordinates. Since all data are now in the same parameter space, additional data from different views can be merged into one data set by simple averaging in the overlapping areas.

It has been observed that the shape of breasts is topologically similar to a hemispherical shape. A breast-centered spherical coordinate system is used in our surface resampling process for integrating 3D data generated from different views.

In order to make the calculation simpler, the new object-centered coordinate system should be placed at the center of the breast. A circle, drawn on the skin along the boundary of the breast, roughly defines the base of the breast. The center of the

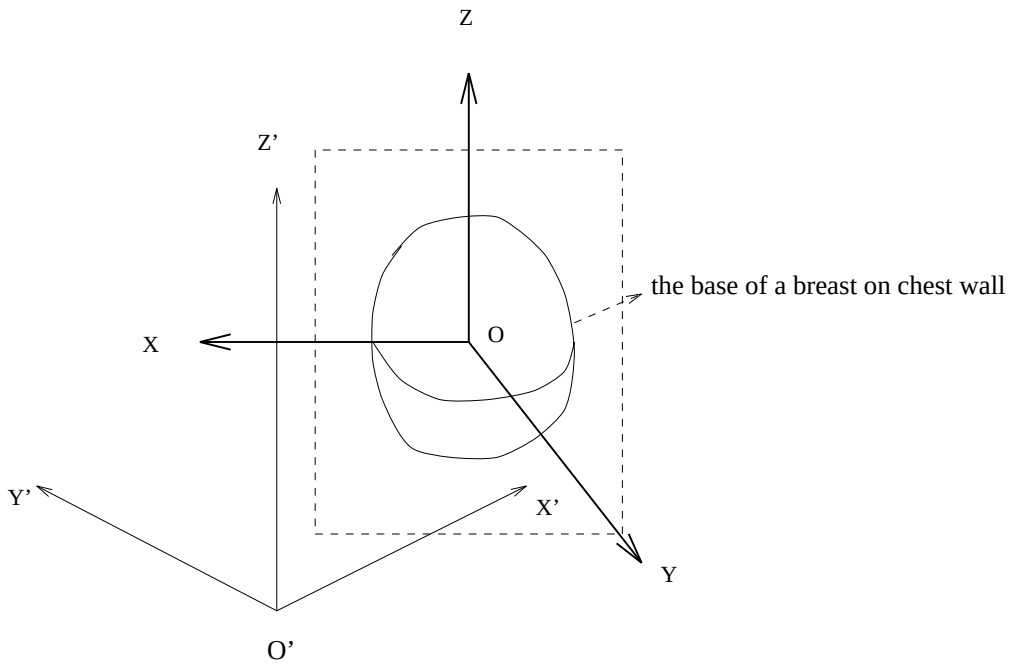

Figure 4.6: Breast-centered coordinate system.

base is taken as the origin of the new coordinate system $OXYZ$, and the base lies on the XZ-plane with the Y-axis pointing out of the chest wall. This is illustrated in Figure 4.6, where $O'X'Y'Z'$ is the original calibration coordinate system, and $OXYZ$ is the new breast centered coordinate system.

3D sample points from each view of the object are transformed from the original coordinate system $O'X'Y'Z'$ to the new system $OXYZ$, and then converted to spherical coordinates. The parameter space is defined by a set of discrete angles of spherical coordinates (ϕ, θ) equally spaced within their ranges ($-\pi/2 \leq \phi \leq \pi/2$) and ($0 \leq \theta < 2\pi$). Each point in the parameter space determines a radial sampling line cast from the origin. The new point on the surface is obtained by finding the intersection of the line and the surface segment. The surface segment is represented by a network of planar triangular facets. Each triangular facet is formed by an interpolation of a plane to a group of three adjacent points. Missing data

Figure 4.7: A cone model surface represented by triangular facets.

areas become holes in the surface segment. Figure 4.7 shows a cone model image represented by triangular facets. This resampling process is repeated for each view and the overlapping points are handled by averaging with a tolerance constraint. If a sampling line does not intersect with any of the surface segments, this surface point is treated as a missing data point.

The SHAPE system generates very dense range data on the object surface thus making it possible to use triangular facets to approximate the surface segment by piecewise linear interpolation. With the two view system, the occlusion problem at the lower part of the breast is largely eliminated, but small regions of missing data points may remain on both the left and right sides. This is improved by using the linear interpolation and the surface fitting technique as described in Chapter 2. Figure 4.8 shows the measurement results using the two view system. A grid of $65(\phi)$x$256(\theta)$ is used in the resampling algorithm where $\Delta\phi$ is 2.8125 and $\Delta\theta$ is 1.40625.

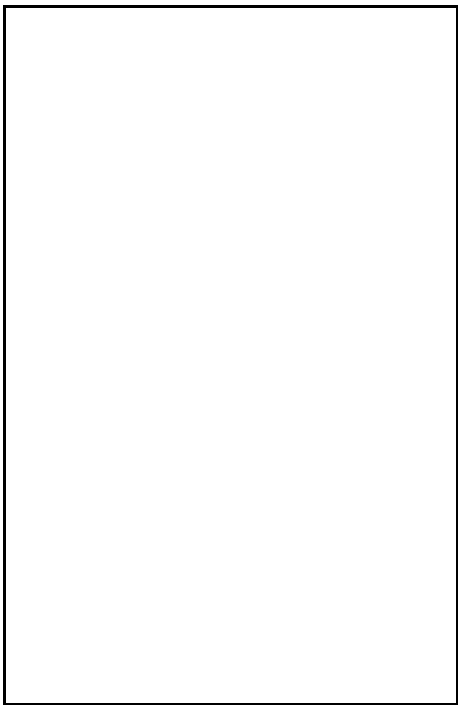

Figure 4.8: Result of the breast model by surface resampling.

4.5 Breast Volume Estimation

A method for breast volume estimation has been used in the CBM system as described in Section 2.3.3. The method deals with the surface data from a single viewpoint and requires the surface sample be determined by a particular position of the projector (parallel to the horizon). It is found that the method can not be applied to estimate the volume from the merged data since the resampled surface is not determined by the position and orientation of the light source.

The standard techniques of numerical integration from data first approximate or interpolate to the 3D data a function possessing the desired degree of smoothness, and then apply the standard numerical integration formulae (e.g. the Newton-Cotes formulas, Romberg's method and Simpson's adaptive quadrature [40]) to compute the integral of the interpolating or approximating function. For example, if cubic splines with continuity constraints are used, C^2 smoothness is obtained. A problem is that if we interpolate the data with a function of higher order smoothness than

present in the data itself, unwanted oscillations occur which may bias the volume estimation.

Using the two view system, most of the surfaces of the breast are covered and missing data areas are limited to small regions which are solved by the linear interplation and the surface fitting techniques as described in Chapter 2. We therefore consider the data itself possessing C^0 smoothness and choose to use interpolating functions having the same degree of smoothness as the data itself. We use triangular facets to interpolate the merged data for the volume estimation.

The volume of the triangular facet surface is calculated as the summation of elementary volumes of the type illustrated in Figure 4.9. The elementary volume is bounded by the origin of the spherical coordinate and two triangular facets representing the surface inside one unit square of the spherical coordinate grid. The volume V of the volume element in Figure 4.9 is computed by decomposing the element into two triangular pyramids or tetrahedra. We have $V = V_p(O, A, B, D) + V_p(O, B, C, D)$ where $V_p(P_1, P_2, P_3, P_4)$ denotes the volume of the pyramid with vertices $P_1(x_1, y_1, z_1)$, $P_2(x_2, y_2, z_2)$, $P_3(x_3, y_3, z_3)$, and $P_4(x_4, y_4, z_4)$. The volume of each pyramid can be calculated using the standard formula $V_p = B * h/3$ where B is the area of the base triangle and h is the height of the pyramid, or computed by the determinant [49]:

$$V_p = 1/6 \begin{vmatrix} x_1 & y_1 & z_1 & 1 \\ x_2 & y_2 & z_2 & 1 \\ x_3 & y_3 & z_3 & 1 \\ x_4 & y_4 & z_4 & 1 \end{vmatrix}.$$

4.6 Experimental Results

The two view system has been used for volume measurements on both stationary objects such as breast models and human breasts for lactating mothers and pregnant women.

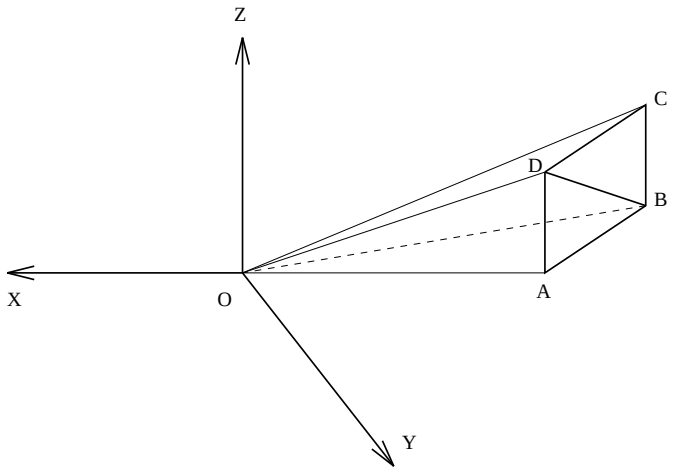

Figure 4.9: Triangular pyramid volume elements.

The two view system works as follows. First, the two camera/projector pairs are calibrated in a global coordinate space. Then, two surface segments with partially overlapped areas are obtained by sequential data acquisition. 3D data points at each view are submitted for the breast boundary detection, possibly pruning and smoothing to obtain the surface segment as described in Chapter 2. Finally, all surface segments are combined and resampled to give the integrated data as the input of the volume calculation program.

A more accurate and efficient step for the mother repositioning herself has been developed in the two view system. A pre-existing image of the breast with a black circle and positioning marks drawn on the skin, which can be an intensity image obtained in the first measurement, is displayed on the monitor. The mother aligns herself at the subsequent measurements by matching the position of the black circle and the repositioning marks in the live image with the black circle and the repositioning marks on the pre-existing image. The use of a pre-existing image assists the mother to reposition herself not only for each experimental section of a set of measurements, but also for different sections of measurements. A JVC KM-1200 colour special effects generator is used to mix a pre-existing image with a live scene.

At each experimental section, a set of separate measurements is performed and the

mean volume (μ) from the set of measurements is taken as the volume for each section. In the meantime, several statistical data are also calculated to describe the precision of the set of measurements which are standard deviation (σ), coefficient of variation (CV), standard error of mean (SEM) and the difference between the maximum and the minimum volume (RANGE).

The following sections give the results of the volume measurement on the breast model as displayed in the previous sections and the results of the breast volume measurements on three lactating mothers.

4.6.1 Experiments of Breast Models

The volume of the model is obtained by calculating the mean value of 9 sets of volume measurements. The calculation is performed, respectively, using the data from the first viewpoint, the second viewpoint and the merged data. The occluded regions are approximated in the volume calculation by linear interpolation and quadratic surface fitting as described in Section 2.4. The volume of the model is also measured using a water displacement method in which the model is placed into a water-filled container. Since the volume of water in the container is known, the volume of the model is obtained from the water displaced. Table 4.1 shows the results. It is noticed from the results that if the water displacement measurement is taken as ground truth, the volume calculated from the merged data is the best estimation in comparison with the volume calculated from the data at either the first or the second viewpoint. Furthermore, the precision of the section of volume measurement is improved using the merged data in terms of the statistical data.

4.6.2 Experiments of Human Breasts

This section describes the experiments of the human breast volume measurements on three lactating mothers. The breast volume is measured before and after a breast-feed. In the meantime, the mother is weighed before and after each breast-feed in

Data	Approx. occluded regions	N	μ	σ	CV (%)	SEM	RANGE
1st view	linear interpolation	9	786.10	1.28	0.16	0.43	4.27
	surface fitting	9	789.68	0.90	0.11	0.30	2.56
2nd view	linear interpolation	9	763.95	4.81	0.63	1.60	14.92
	surface fitting	9	769.09	1.65	0.21	0.55	5.27
merged	linear interpolation	9	742.23	0.67	0.09	0.22	2.23
	surface fitting	9	741.67	0.64	0.09	0.21	2.11
water displacement		8	738.75	7.55	1.02	2.67	20.00

Table 4.1: Results of the volume measurement on the breast model (ml).

order to obtain an independent measure of milk exchange between the mother and her infant. The methods used to convert milk exchange from weight to volume are the same as the methods used by the CBM system as described in Chapter 2. 30 sections of experiments are performed. For each section, the mean breast volume is calculated from a set of between three and ten separate measurements. Using the 30 sections of measurements, the intrasection C.V is found to average 1.16%. Breast volume measurements for the three lactating mothers range from approximately 550 ml to 1100 ml.

We compared the change in breast volume before and after a breast-feed (y) as measured by the two view system to the amount of milk removed by the infant at that breast-feed (x) as measured by test weighing. The linear regression $y = 0.98x - 4.01$ ($r = 0.97$, $n = 14$) describes the relationship between the two methods of determining milk exchange as shown in Figure 4.10. A similar linear regression $y = 1.05x - 1.79$ ($r = 0.95$, $n = 14$) is obtained by using the CBM system.

The results of the linear regression obtained from the CBM system and the two view system may not show much difference. However, the information on the breast surface generated by the two view system is significantly more complete than the CBM system can provide. Table 4.3, 4.4 and 4.5 show the results of the number of missing

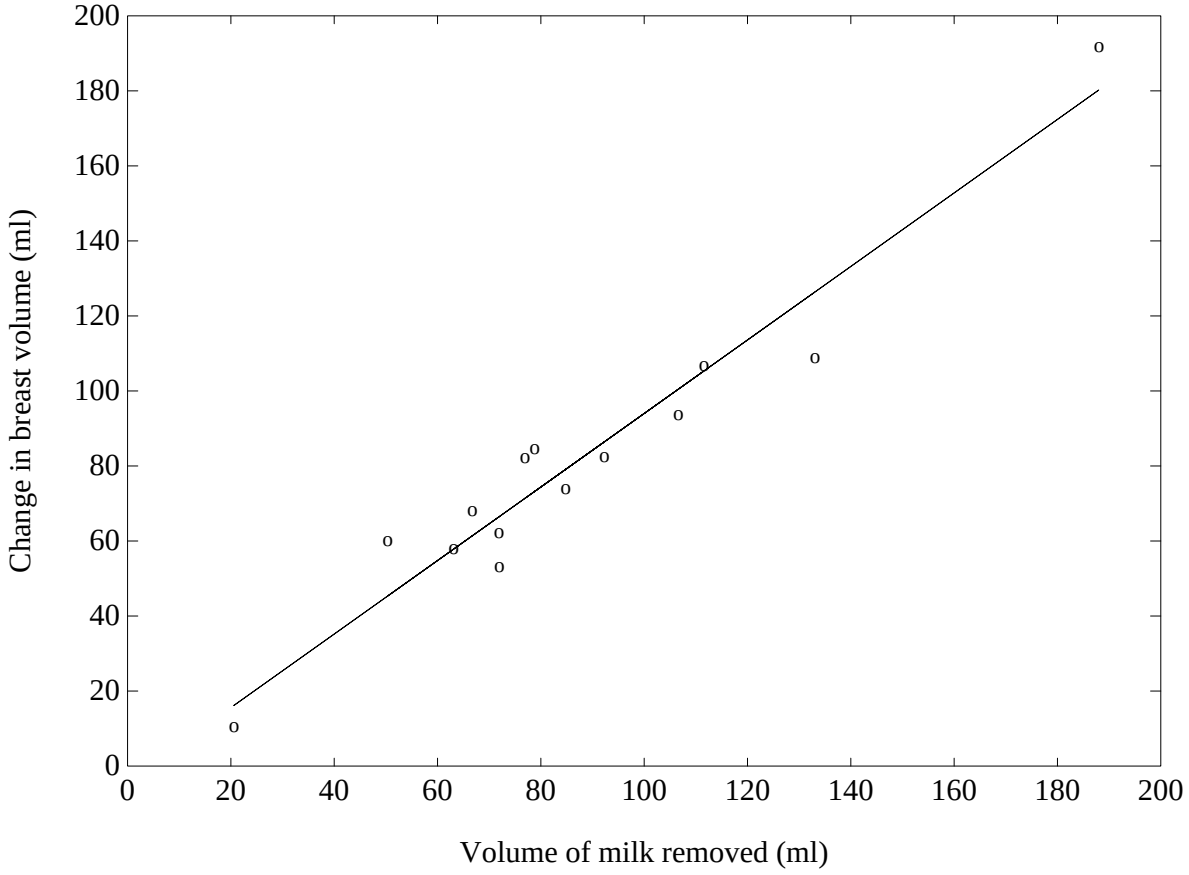

Figure 4.10: The relationship between the volume of milk removed by the infant at a breast-feed, measured by test weighing (abscissa), and the change in breast volume, measured by the two view system (ordinate).

System	σ	CV (%)	SEM	RANGE
CBM	12.88	1.47	4.51	39.79
Two-view	8.44	1.16	3.02	25.09

Table 4.2: The averaged statistical data of 30 sections generated by the CBM system and the two view system.

Side	Data	Sections	Missing data areas (%)
Right	1st view	6	16.78
	2nd view	6	34.44
	Merged	6	6.99
Left	1st view	6	18.01
	2nd view	6	23.86
	Merged	6	7.36

Table 4.3: Results of the breast surface measurement of Mother A.

data points on the breast surface generated, respectively, from the measurement of the first viewpoint, the second viewpoint and the merged data. Furthermore, since more surface data are obtained from the two viewpoints, similar to the experiment on the breast model, the precision of the volume measurement is improved in terms of standard deviation, coefficient of variation, standard error of the mean and the difference between the maximum and the minimum volume in a set of separate measurements. Table 4.2 shows the difference of the statistical data of breast volume measurements using the two systems. These data are produced by averaging the statistical data of the 30 sections of the breast volume measurements on the three lactating mothers.

Side	Data	Sections	Missing data areas (%)
Right	1st view	6	16.47
	2nd view	6	27.15
	Merged	6	5.66
Left	1st view	2	26.30
	2nd view	2	26.69
	Merged	2	14.29

Table 4.4: Results of the breast surface measurement of Mother B.

Side	Data	Sections	Missing data areas (%)
Right	1st view	8	28.09
	2nd view	8	26.94
	Merged	8	13.80
Left	1st view	2	24.77
	2nd view	2	25.13
	Merged	2	8.83

Table 4.5: Results of the breast surface measurement of Mother C.

4.7 Discussion

The results have shown that the two view system can be used to accurately measure the breast surface and thus determine changes in the volume of milk contained within the breast by comparing the change in breast volume before and after a breast-feed with the volume of the milk removed by the infant. In addition, more complete information on the breast surface is recovered by using the two view system. The more complete surface information not only improves the accuracy of the volume measurement, but also provides a basis for high level representation of the surface. Therefore this system assists further research on human lactating such as the change in breast surface over short periods of time between breast feeds, or the development of lactation during pregnancy and immediately after the birth of a child.

Using the two view system, the occlusion problem at the lower part of the breast is largely eliminated, but small regions of missing data points can remain on both the left and right sides which are handled by the surface fitting techniques as described in Chapter 2. In order to achieve a more accurate measurement, more than two sensors positioned at corresponding viewpoints are needed for recovering large occluded regions. This may involve 3D registration [19] between views or calibration techniques for multiple sensors [20].

As shown in Figure 4.5, we notice that there is always a slight difference in the overlapping areas caused by calibration errors or by the movement of the object during data acquisition. Currently, overlapping data is handled by equal-weight averaging. More accurate methods may be investigated in the future. The details of error analysis of the SHAPE system are discussed in [3].

4.8 Conclusion

Human observers are very good at recognizing three dimensional objects. However, in computer vision applications, the recovery of 3D surface information still has

certain limitations in terms of accuracy, robustness and speed. A single view is often insufficient to infer global 3D surface properties of the object because of the occlusion problem. Integrating 3D information from multiple views is necessary for a more complete description of the surface of the object. Constraints imposed by applications affect the techniques used. Several approaches for generating multiple view vision systems have been surveyed in this chapter. An implementation of a two view vision system based on stationary sensors is presented.

We have demonstrated that the two view system can be accurately used to measure short-term changes in breast volume for lactating mothers. Currently, the system is also used to observe the breast volume change of pregnant women over many weeks. However, the application of the system is not limited to human body measurement. It also provides a basis for other applications, including engineering applications and CAD, for generating a complete 3D model.

Chapter 5

Conclusion

In this Chapter, we conclude our work by discussing the successes, and limitations of our system and by making suggestions for future research.

Successes

We have developed a simple method for solving occlusion problems in active binocular vision systems and for acquiring images from multiple views simultaneously. Combined with a camera and a projector, a mirror is used in the method to create an additional viewpoint to recover the occluded regions that are illuminated by the light source but were previously invisible to the camera. Using this method, we can achieve a more complete measurement without increasing image capture time (less than one second), which is very useful in applications of measuring biological shapes where both speed and accuracy are important.

We have implemented a two view 3D measurement system based on the SHAPE system. The feasibility of using the two view system for measuring breast surface and volume has been demonstrated by the experimental results described in Chapter 4. Currently, the system is used to observe the breast volume change of pregnant women over many weeks' time. The two view system has the potential to be an important tool in the biochemical study of human lactation. The applications of

the system are not limited to human body measurement. The system also provides a basis for other applications, including engineering applications and CAD, for generating a complete 3D model.

We have implemented a 3D surface resampling algorithm. Using the algorithm, all data from different viewpoints are integrated into an object-centered coordinate space and resampled by a single parametric grid. We have also implemented a numerical method for estimating the breast volume defined by a sample of 3D points on the breast surface.

The SHAPE system has been extended by our work. First, the extended system can overlay a live scene with a pre-stored image. This utility provides an accurate and efficient means to assist the subject in keeping a consistent pose during subsequent measurements over time. Thus, it improves the accuracy of the measurement of volume changes. Second, the extended system has the flexibility to make measurements from two different viewpoints either by using a mirror or by a second camera/projector pair. Finally, we have converted the SHAPE software for 3D measurement from PC platforms to Sun workstation platforms with a new graphical user interface. The Sun-based system improves the speed of data processing and the new graphical user interface is simple and efficient to use.

Limitations and Suggestions for Future Work

Our method of combining a mirror with a camera/projector pair requires that the occluded regions to be recovered should be illuminated by the light source. This requirement results in a limitation on the shapes of objects. For those objects where a single light source fails to illuminate all the regions of interest, this method cannot be applied to recover the regions that the light source cannot "see". This limitation can be solved by using multiple sensors (camera/ projector pairs) at vantage viewpoints at the cost of increasing image acquisition time as described in Chapter 4. In addition, it is also possible to combine active sensors with multiple mirrors used as either virtual sensors or scanning devices in achieving more complete

3D measurements.

The image acquisition time of our two view system is about 6 seconds using a Matrox MVP AT frame grabber connected to a PC-386 computer. The subject must keep still during image acquisition. The time for image acquisition can be reduced if more advanced computers and frame grabbers are used. Our 3D surface resampling algorithm described in Chapter 4 is only suitable for objects with spherical shapes. Investigations of more general methods may be needed for 3D surface reconstruction of objects with arbitrary shapes. The use of the two view system can largely eliminate occlusion regions at the lower part of the breast. Missing data areas still remain on both sides of some large sized breasts. In these cases, more viewpoints are required to obtain a more complete measurement which may involve investigations of approaches for sensor calibration or view registration.

Further development is needed on the study of approaches for evaluating changes in two corresponding surfaces over time, which is very important for biochemical applications. Investigations of methods for 3D registration and pose estimation may be required for the further study.

Appendix A

The SHAPE System

The SHAPE system developed at Monash University [4,3] is a 3D shape measurement system based on a structured lighting triangulation technique. The system is employed in the work of this thesis. This Appendix gives an overview of the system.

A.1 Introduction

The principle of the shape measurement system is based on active triangulation. A beam of light from a projector is used to form a bright spot on the object at a point to which the range is to be measured. A camera displaced at a known distance (the base line) from the light source views the scene. One angle is defined by the beam of light and the base line, and the other is determined by the line specified by the position of the spot of light on the camera's image and the base line. From a knowledge of the base line and the two angles, triangulation can be applied to determine the 3D coordinates of the point on the object [11]. By scanning the light beam at an array of points on the object's visible surface, an overall measurement of the surface can be obtained. Instead of using a beam of light, a more efficient method is to use a sheet of light which forms a light stripe on the surface so that a number of points on the stripe can be measured per frame. The method exploits the fact that in three dimensions a point may be specified by the intersection of a

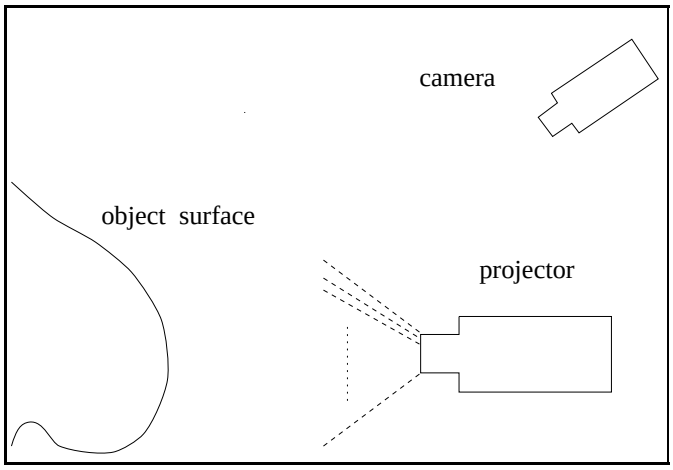

Figure A.1: Camera and projector arrangement in the SHAPE system.

line and a plane.

In both the light stripe and the single dot approach, the projected light must be scanned for an overall measurement to be made. The need for scanning may be avoided by the projection of a pattern of structured light such as an array of dots, a set of stripes or a grid simultaneously onto the scene. However, it is necessary to establish the correspondence between each of the light spots or stripes in the camera's image and its corresponding projected light from the light source. 3D coordinates of points on the illuminated portions of the surface can then be determined by triangulation.

The SHAPE system uses a liquid crystal light valve mounted in a projector to code an array of 64 horizontally projected stripes. These 64 stripes are projected in a sequence of six coded patterns in which the intensity (on or off) of each stripe in a pattern indicates the value of the respective bit of the code for the corresponding stripe. A single camera views the scene from above the projector. Figure A.1 shows the system arrangement. An example of the measurement of a cone model using the system is shown in Figure A.2.

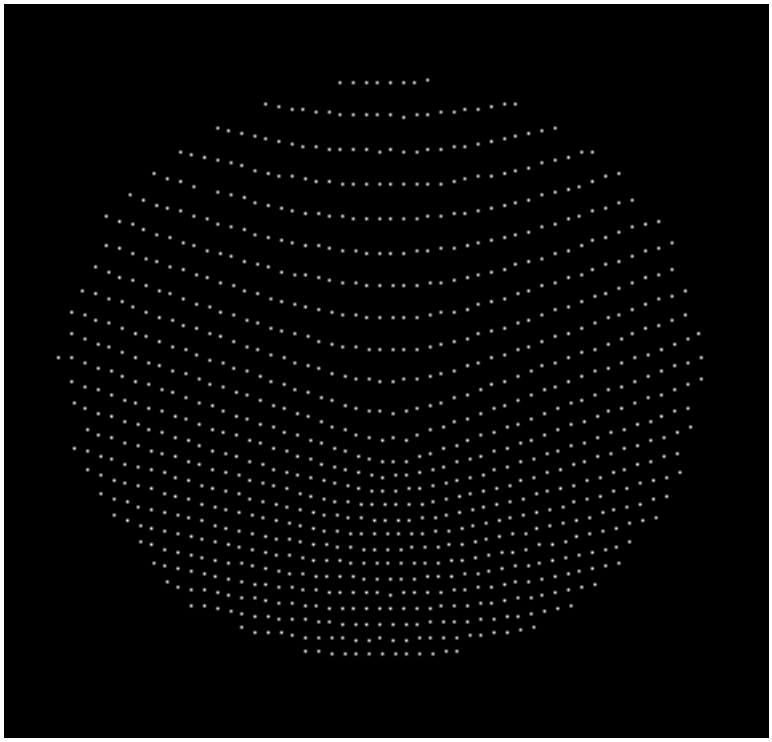

Figure A.2: An example of a point display of measured 3D data.

A.2 Overview of the SHAPE System

A calibration process must be performed beforehand to allow accurate transformation from the stripe code to the equation of the corresponding light plane (projector calibration) and from the camera image coordinates to the equation of the corresponding line (camera calibration).

An object to be measured is placed in the space previously occupied by a calibration frame. Eight images (one with all stripes on, one with all stripes off and six coding patterns) are captured by a CCD camera. These images are then processed automatically by the system to calculate the 3D coordinates of sample points on the visible surface of the object.

The process of the shape measurement consists of the following steps [3]. A brief description of each of these steps is given in the following sections.

- Location of points at the centers of the projected stripes in the camera's image.

These points are the sample points on the surface for which the 3D coordinates will be determined.

- Identification of the stripes via the coding process which involves using the light valve to modulate the intensity of the stripes.
- Calculation of the coordinates of the sample points by triangulation.

A.2.1 Stripe Location

Stripe location is a process of edge detection which extracts stripe features in a reference image.

The reference image is created by removing the ambient component of scene illumination through subtracting the image taken with all the stripes turned off from the image with all the stripes turned on. The stripes are accurately located in the reference image. Since the camera is offset vertically from the projector and the stripes are projected horizontally the stripes appear generally horizontal in the camera's image. A plot of intensity along a column of the image will therefore generally show a well defined peak in intensity wherever a stripe intersects the column.

The stripe location algorithm uses the first derivative to locate all the local maxima and minima of the intensity profile along a column of the image. A series of rules are then applied to distinguish valid rises and falls in intensity from those caused by electronic noise or surface reflectance variations. After the location of the pixels corresponding to the stripe is found, the centroid of the intensity profile is used to estimate the vertical position of the stripe center to sub-pixel accuracy.

A.2.2 Stripe Coding

Stripe coding is a process of matching each of the light stripes in the camera's image with the corresponding projected light from the light source.

The SHAPE system uses an approach based on coded binary patterns [11] by illu-

minating the scene with a sequence of six coded light patterns. An image is taken for each of the patterns. The intensity of each stripe in the six coded light patterns indicates the values of the respective bits in its code. The coding algorithm works as follows. The intensity of the pixels in the coding image at the coordinates of each of the previously located stripe centers is compared with the corresponding pixels in the reference image as described above. If the intensity in the coding image is greater than half that in the reference image the stripe is assumed to be on and the code bit for the pixel is set to one, otherwise it is set to zero. The background image is subtracted from each coding image beforehand. The algorithm is able to detect situations where coding errors occur and remove such points from further consideration.

An example of a cone model illuminated by the sequence of patterns is shown in Figure A.3 for bit 0 to bit 5 from (a) to (f). The stripes are coded 0 to 63 from top to bottom.

A.2.3 Triangulation and Calibration

Figure A.4 shows the active triangulation geometry used in the SHAPE system. The camera views a point P which lies at the center of a projected stripe. The image of P is at coordinates x_i^c, y_i^c on the camera's image. The light stripe has code (projector's image coordinate) y_i^p. The coordinates x_i^c and y_i^c specify a line which is known to pass through P and the coordinate y_i^p specifies the plane passing through P defined by the projected light stripe.

Camera and projector calibration are used to find the parameters of the camera and projector models which, given the image coordinates x_i^c, y_i^c and y_i^p, allow the equations of this line and plane to be determined. The 3D coordinates P can then be determined by finding the intersection of the line and plane.

If a range measurement system is to be successful, accurate estimation of camera parameters is of paramount importance. The DLT (Direct Linear Translations) method [1] is implemented in the SHAPE system for both camera and projector

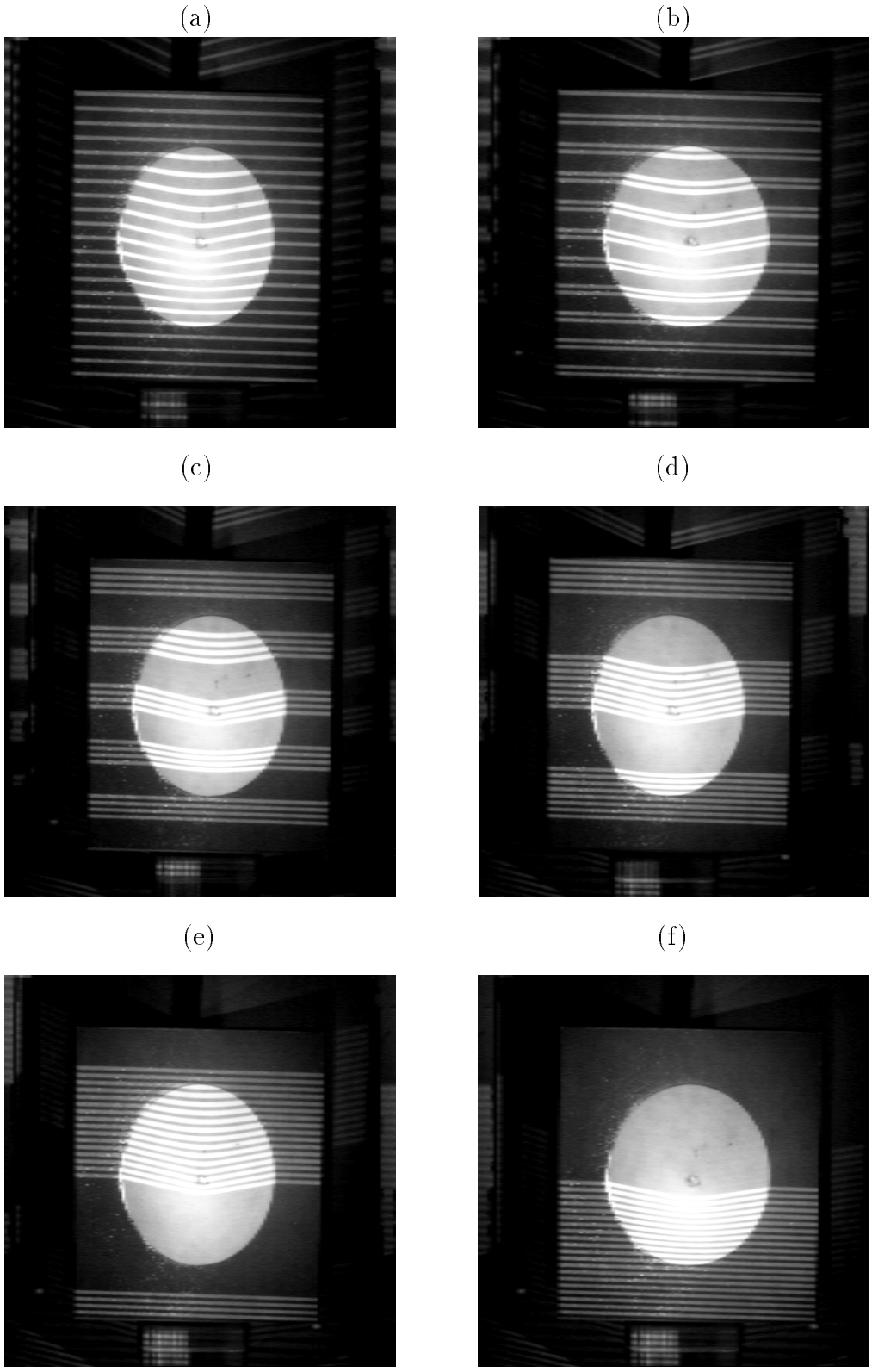

Figure A.3: Coding patterns.

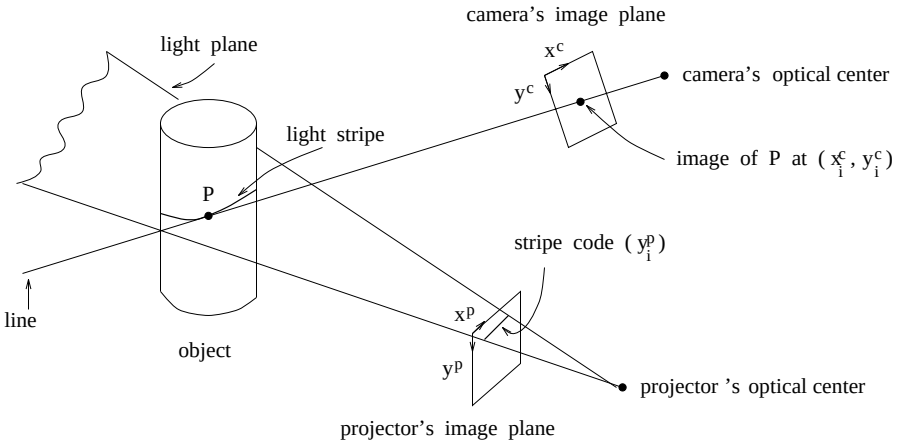

Figure A.4: Active triangulation geometry.

calibration. The camera is modelled using the following two equations which relate the world coordinates X, Y, Z of a point to the image coordinates x_i^c and y_i^c as a function of the composite parameters C_{ij}, $1 \leq i \leq 3$, $1 \leq j \leq 4$. Camera calibration determines the 11 parameters C_{11} to C_{33} ($C_{34} = 1$).

$$x_i^c = \frac{C_{11}X + C_{12}Y + C_{13}Z + C_{14}}{C_{31}X + C_{32}Y + C_{33}Z + 1} \quad \text{(A.1)}$$

$$y_i^c = \frac{C_{21}X + C_{22}Y + C_{23}Z + C_{24}}{C_{31}X + C_{32}Y + C_{33}Z + 1} \quad \text{(A.2)}$$

The projector is modelled by the following equation which relates the world coordinates of a point to the y image coordinate y_i^p (stripe code) of the stripe on which the point lies. Projector calibration determines 7 parameters P_{21} to P_{33}.

$$y_i^p = \frac{P_{21}X + P_{22}Y + P_{23}Z + P_{24}}{P_{31}X + P_{32}Y + P_{33}Z + 1} \quad \text{(A.3)}$$

Equations (A.1) and (A.2) can be arranged to give the following equivalent equations respectively.

$$C_{11}X + C_{12}Y + C_{13}Z + C_{14} - C_{31}Xx_i^c - C_{32}Yx_i^c - C_{33}Zx_i^c = x_i^c \quad \text{(A.4)}$$

$$C_{21}X + C_{22}Y + C_{23}Z + C_{24} - C_{31}Xy_i^c - C_{32}Yy_i^c - C_{33}Zy_i^c = y_i^c \quad \text{(A.5)}$$

The camera calibration is implemented using an image of a number of target points with precisely known world coordinates. Each target point gives the two linear

equations (A.4) and (A.5) in the 11 unknowns C_{11} and C_{33}. Six or more target points will give 12 or more such equations. The system of equations will be overdetermined so a least squares solution is used for C_{11} to C_{33}. In practice, the world coordinate system is defined by a calibration frame and 12 known target points are used for the camera calibration.

The projector calibration is similar to the camera calibration. Equations (A.3) can be arranged to give

$$P_{21}X + P_{22}Y + P_{23}Z + P_{24} - P_{31}Xy_i^p - P_{32}Yy_i^p - P_{33}Zy_i^p = y_i^p \quad \text{(A.6)}$$

Seven or more points on stripe centers with known world coordinates and known projector y image coordinates (stripe code) will give seven or more equations of (A.6) allowing solution for the unknown P_{21} to P_{33}. More details of the implementation are contained in [3].

A.3 Accuracy

Measurement accuracy is defined as the agreement between the measured coordinates of a sample point on a surface and the true value of the coordinates. Measurement precision is the variation between measurements in a set of measurements of the same sample point on a surface. The system's measurement accuracy is analysed in detail in [3]. The following results were reported in [3]. There are two fundamental sources of measurement error:

- The error in location of the light stripes in the camera's image.
- The error in calibration of the camera and projector.

Estimation of the 2D position of the center points on the light stripes is done by calculating the centroid of the intensity profile of the stripe in the camera's image. This technique is widely used for location of features in images to sub-pixel accuracy. Error due to noise was measured to be about 0.02 pixels at high image intensities.

The main aspect of the accuracy of DLT calibration is the way in which the error in calibration varies over the measurement volume and depends on the distribution of, and error in, the calibration target points. In the volume spanned by the calibration target points the error in calibration was of the same order as the error in the coordinates of the target points. Outside this volume the error increased.

A statistical technique was used for estimation of variation of the calibration error over the measurement volume. An accuracy of 1:3100 of the field of view of the projector was obtained using the technique for an angle of 33 degrees between the camera and the projector.

The measurement precision was estimated as 1:12000 of the camera's field of view using the measured error in stripe center location due to noise of 0.02 pixels and assuming an angle of 30 degrees between the camera and the projector.

Bibliography

[1] Y. I. Abdel-Aziz and H. M. Karara. Direct Linear Transformation from Comparator Coordinates into Object Space Coordinates in Close-Range Photogrammetry. In *Proc. Symposium on Close Range Photogrammetry*, pages 1–18, Urbana, Illinois, January 1971.

[2] N. Ahuja and J. Veenstra. Generating Octrees from Object Silhouettes in Orthographic Views. *IEEE Transactions on Pattern Analysis and Machine Intelligence*, 11(2):137–149, February 1989.

[3] B. F. Alexander. *High Accuracy Non-Contact Three Dimensional Shape Measurement.* PhD thesis, Monash University, Australia, 1989.

[4] B. F. Alexander and K. C. Ng. 3D Shape Measurement by Active Triangulation Using an Array of Coded Light Stripes. In *Proc. SPIE: Optics, Illumination and Image Sensing for Machine Vision II*, volume 850, pages 199–209, November 1987.

[5] P. G. Arthur. *Novel Methods for Milk Synthesis in Lactating Mothers.* PhD thesis, The University of Western Australia, 1988.

[6] P. G. Arthur, P. E. Hartmann, and M. Smith. Measuring Milk Intake of Breast-Fed Infants. *Journal of Pediatric Gastroenterology and Nutrition*, 6:758–763, 1987.

[7] P. G. Arthur, T. J. Jones, J. Spruce, and P. E. Hartmann. Measuring Short-Term Rates of Milk Synthesis in Breast-Feeding Mothers. *Quarterly Journal of Experimental Physiology*, 74:419–428, 1989.

[8] N. Ayache and B. Faverjon. Efficient Registration of Stereo Images by Matching Graph Descriptions of Edge Segments. *International Journal of Computer Vision*, 1(2):107–131, 1987.

[9] D. H. Ballard and C. M. Brown. *Computer Vision.* Prentice-Hall, Englewood Cliffs, New Jersey, 1982.

[10] G. Beheim and K. Fritsch. Ranging Finding Using Frequency-modulated Laser Diode. *Applied Optics*, 25(9):1439–1442, May 1986.

[11] P. J. Besl. Active Optical Range Imaging. In J. L. G. Sanz, editor, *Advances in Machine Vision*, pages 1–63. Springer-Verlag, 1989.

[12] B. Bhanu. Representation and Shape Matching of 3D Objects. *IEEE Transactions of Pattern Analysis and Machine Intelligence*, 6(3):340–351, May 1984.

[13] A. Blake, D. McCowen, H. R. Lo, and P. J. Lindsey. Trinocular Active Range-Sensing. *IEEE Transactions on Pattern Analysis and Machine Intelligence*, 15(5):477–483, May 1993.

[14] S. H. Boey. *High Accuracy Three-Dimensional Model Generation.* PhD thesis, Monash University, Australia, 1990.

[15] R. M. Bolle and B. C. Vemuri. On Three-Dimensional Surface Reconstruction Methods. *IEEE Transactions on Pattern Analysis and Machine Intelligence*, 13(1):1–13, January 1991.

[16] R. C. Bolles, J. H. Kremers, and R. A. Cain. A Simple Sensor to Gather Three-Dimensional Data. Technical Report 249, Stanford Research Institute, July 1981. SRI Project 1538.

[17] M. I. Bullock and I. A. Harley. The Measurement of Three-Dimensional Body Movements by the Use of Photogrammetry. *Ergonomics*, 15(3):309–322, 1972.

[18] C. E. Casey, K. M. Hambidge, and M. C. Neville. Studies in Human Lactation: zinc, copper, manganese and chromium in human milk in the first month of lactation. *American Journal of Clinical Nutrition*, 41:1193–1200, 1985.

[19] Y. Chen and G. Medioni. Object Modelling by Registration of Multiple Range Images. *Image and Vision Computing*, 10(3):145–155, April 1992.

[20] C. C. Cheung, B. F. Alexander, W. A. Brown, and K. C. Ng. Relative Camera Calibration. In *Proceedings of the IEEE International Conference on Image Processing*, pages 461–465, Singapore, September 1989.

[21] C. H. Chien, Y. B. Sim, and J. K. Aggarwal. Generation of Volume/Surface Octree from Range Data. In *Proceedings of CVPR'88*, pages 254–260, Ann Arbor, Michigan, June 1988.

[22] S. Daly, J. Kent, D. Huynh, R. Owens, B. F. Alexander, K. C. Ng, and P. E. Hartmann. The Determination of Short-Term Breast Volume Changes and the Rate of Synthesis of Human Milk Using Computerized Breast Measurement. *Quarterly Journal of Experimental Physiology*, 77(1):70–87, January 1992.

[23] S. Daly, R. Owens, and P. E. Hartmann. The Short-Term Synthesis and Infant-Regulated Removal of Milk in Lactating Women. *Quarterly Journal of Experimental Physiology*, 78(2):209–220, March 1993.

[24] P. L. Dimatteo, J. A. Ross, and H. K. Stern. Arrangement for Sensing the Geometric Characteristics of an Object. *United States Patent*, November 1979.

[25] D. A. Dixon and I. Newton. Minimal Forms of the Cleft Syndrome Demonstrated by Stereophotogrammetric Surveys of the Face. *British Dental Journal*, 132:183–189, 1972.

[26] F. P. Ferrie and M. D. Levine. Integrating Information from Multiple Views. In *Proceedings of IEEE Workshop on Computer Vision*, pages 117–122, Miami Beach, Florida, November-December 1987.

[27] W. Frobin and E. Hierholzer. Automatic Measurement of Body Surfaces Using Rasterstereography. *Photogrammetric Engineering and Remote Sensing*, 49(3):377–384, March 1983.

[28] Y. Ge and R. Owens. 3D Shape Measurement Using Multiple Structured Images and a Mirror. In *Proceedings of the 1992 Department Research Conference,*

The Department of Computer Science, The University of Western Australia, Perth, Australia, July 1992.

[29] Y. Ge, R. Owens, and P. E. Hartmann. Breast Volume Measurement from Multiple Views. In *Proceedings of First Australian and New Zealand Conference on Intelligent Information Systems*, pages 339–343, Perth, Australia, December 1993.

[30] W. Gellert, S. Gottwald, M. Hellwick, H. Kästner, and H. Küstner, editors. *The VNR Concise Encyclopedia of Mathematics*. Van Nostrand Reinhold, New York, second edition, 1989.

[31] L. A. Gerhardt and W. I. Kwak. An Improved Adaptive Stereo Ranging Method for Three-Dimensional Measurements. In *Proceedings of CVPR'86*, pages 21–26, Miami Beach, Florida, June 1986.

[32] E. L. Hall, J. K. B. Tio, C. A. McPherson, and F. A. Sadjadi. Measuring Curved Surfaces for Robot Vision. *Computer*, pages 42–54, December 1982.

[33] J. G. Hall, U. G. Froster-Iskenius, and J. E. Allanson. *Handbook of Normal Physical Measurements*. Oxford University Press, 1989.

[34] P. E. Hartmann. The Breast and Breast-Feeding. In E. Philipp and M. Setchell with J. Ginsburg, editors, *Scientific Foundations of Obstetrics and Gynaecology*, pages 378–390. Oxford Butter-Worth Heinemann, 4th edition, 1991.

[35] P. E. Hartmann and L. Saint. Measurement of Milk Yield. *Journal of Pediatric Gastroenterology and Nutrition*, 3:270–274, 1984.

[36] B. K. P. Horn. *Robot Vision*. The MIT Press, 1986.

[37] D. Huynh, R. Owens, S. Daly, J. Kent, and P. E. Hartmann. The Occlusion Problem in Breast Volume Measurement. In *The 4th Australian Joint Artificial Intelligence Conference*, pages 653–666, November 1990.

[38] D. Huynh, R. Owens, S. Daly, J. Kent, and P. E. Hartmann. The Rapid Estimation of Short Changes in Breast Volume. In *The 6th International Conference on Biomedical Engineering*, pages 93–96, Singapore, December 1990.

[39] F. E. Hytten. Clinical and Chemical Studies in Human Lactation. VI. The Functional Capacity of the Breast. *British Medical Journal i*, pages 912–915, 1954.

[40] I. Jacques and C. Judd. *Numerical Analysis*. Chapman and Hall, 1987.

[41] R. A. Jarvis. A Perspective on Range Finding Techniques for Computer vision. *IEEE Transactions of Pattern Analysis and Machine Intelligence*, 5(2):122–139, 1983.

[42] P. R. M. Jones, G. M. West, D. H. Harris, and J. B. Read. The Loughborough Anthropometric Shadow Scanner (LASS). *Endeavour, New Series*, 13(4):162–168, 1989.

[43] M. Kass, A. Witkin, and D. Terzopoulos. Snakes: Active Contour Models. *International Journal of Computer Vision*, 1(4):321–331, January 1988.

[44] R. L. Keizer. *A Structured Light System and its Use for Noncontact 3D Measurement of the Human Body Surface*. PhD thesis, Rutgers The University of New Jersey, New Brunswick, 1991.

[45] Y. C. Kim and J. F. Aggarwal. Rectangular Parallelepiped Coding: A Volumetric Representation of Three Dimensional Objects. *IEEE Journal of Robotics and Automation*, 2(3):127–134, September 1986.

[46] M. D. Levine, D. A. O'Handley, and G. M. Yagi. Computer Determination of Depth Maps. *Computer Graphics and Image Processing*, 2:134–150, 1973.

[47] R. A. Lewis and A. R. Johnston. A Scanning Laser Rangefinder for a Robotic Vehicle. In *Proc. 5th International Joint Conference on Artificial Intelligence*, pages 762–768, August 1977.

[48] G. Loopuyt and M. Blaustein. A New Equipment for Photogrammetric Acquisition of Facial Data. In *PROC. Biostereometrics'85*, volume 602, pages 34–39, 1985.

[49] A. L. Mackay. The Numerical Geometry of Biological Structrues. In M. J. Geisow and A. N. Barrett, editors, *Computing in Biological Science*, pages 349–392. Elsevier Biomedical Press, 1983.

[50] R. Martin and K. Saller. *Lehrbuch der Anthropologie*. Gustav Fischer Verlag, Stuttgart, 1962.

[51] G. Medioni and R. Nevatia. Segment-based Stereo Matching. *Computer Graphics and Image Processing*, 31:2–18, 1985.

[52] M. Milles, P. J. Desjardins, and H. E. Pawel. The Facial Plethysmograph: a New Instrument to Measure Facial Swelling Volumetrically. *Journal of Oral and Maxillofacial Surgery*, 43:346–352, 1985.

[53] R. Mollard, M. Sauvignon, and C. Pineau. Biostereometric Study of a Sample of 50 Young Adults by Photogrammetry. In *PROC. Biostereometrics'82*, pages 234–240, 1982.

[54] I. F. K. Muir, T. L. Barclay, and A. D. Settle. *Burns and their Treatment.* Butterworths, London, 1987.

[55] J. L. Mundy and G. B. Porter III. A Three-Dimensional Sensor Based on Structured-Light. In T. Kanade, editor, *Three-Dimensional Machine Vision*, pages 3–61. Kluwer Academic Publishers, 1987.

[56] M. C. Neville and M. R. Neifert, editors. *LACTATION Physiology, Nutrition and Breast-Feeding.* Plenum Press, New York, 1983.

[57] D. Nitzan, R. Bolls, and R. O. Duda. The Measurement and Use of Registered Reflectance and Range Data in Scene Analysis. *Proceedings of IEEE*, 65(2):206–220, 1977.

[58] H. Noborio, S. Fukuda, and S. Arimoto. Construction of the Octrees Approximating Three-Dimensional Objects by Using Multiple Views. *IEEE Transactions on Pattern Analysis and Machine Intelligence*, 10(6):769–782, November 1988.

[59] M. Oshima and Y. Shirai. Object Recognition Using Three-Dimensional Information. *IEEE Transactions on Pattern Analysis and Machine Intelligence*, 5(4):353–361, July 1983.

[60] J. L. Posdamer and M. D. Altschuler. Surface Measurement by Space-encoded Projected Beam Systems. *Computer Graphics and Image Processing*, 18:1–17, 1982.

[61] M. Potmesil. *Generating Three-Dimensional Surface Models of Solid Objects from Multiple Projections.* PhD thesis, Rensselaer Polytechnic Institute, 1982.

[62] D. Poussart and D. Laurendeau. 3-D Sensing for Industrial Computer Vision. In J. L. G. Sanz, editor, *Advances in Machine Vision*, pages 122–159. Springer-Verlag, 1989.

[63] A. Prentice, A. Paul, A. Black, T. Cole, and R. Whitehead. Cross-cultural Difference in Lactation Performances. In M. Hamosh and A. S. Goldman, editors, *Human Lactation 2: Maternal and Environmental Factors*, pages 13–14. Plenum Press, New York, 1986.

[64] A. K. I. Torlegård. Body Measuring System with Analytical Stereophotogrammetry through Mirrors. In *Symposium on Close-Range Photogrammetric Systems*, pages 236–244, Champaign, Illinois, 1975.

[65] I. Reid. Measuring Short-Term Changes in Breast Volume Using Raster Stereometry. Technical report, Department of Computer Science, The University of Western Australia, November 1988. TR 88/11.

[66] I. Reid and M. Brady. Model-based Recognition and Range Imaging for a Guided Vehicle. *Image and Vision Computing*, 10(3):197–207, April 1992.

[67] M. Rioux. Laser Range Finder based on Synchronized Scanners. *Applied Optics*, 23(21):3837–3844, November 1984.

[68] P. Saint-Marc, J. L. Jezouin, and G. Medioni. A Versatile PC-Based Ranging Finding System. *IEEE Transactions on Robotics and Automation*, 7(2):250–256, April 1991.

[69] Y. Sato, H. Kitagawa, and H. Fujita. Shape Measurement of Curved Objects Using Multiple Slit-Ray Projections. *IEEE Transactions of Pattern Analysis and Machine Intelligence*, 4(6):641–646, November 1982.

[70] Y. Shirai and M. Suwa. Recognition of Polyhedrons with a Range Finder. In *Second International Joint Conference on Artificial Intelligence*, pages 80–87, Imperial College, London, September 1971.

[71] M. R. Stytz, G. Frieder, and O. Frieder. Three-Dimensional Medical Imaging: Algorithms and Computer Systems. *ACM Computing Surveys*, 23(4):421–499, December 1991.

[72] J. P. Trevelyan. *Robots for Shearing Sheep : Shear Magic*. Oxford University Press, 1992.

[73] R. Y. Tsai. An Efficient Accurate Calibration Technique for 3D Machine Vision. In *Proceedings of CVPR'86*, pages 364–374, Miami Beach, Florida, June 1986.

[74] M. W. Vannier, T. Pilgram, G. Bhatia, B. Brunsden, and P. Commean. Facial Surface Scanner. *IEEE Computers and Applications*, pages 72–80, November 1991.

[75] B. C. Vemuri and J. K. Aggarwal. 3-D Model Construction from Multiple Views and Intensity Data. In *Proceedings of CVPR'86*, pages 435–437, Miami Beach, Florida, June 1986.

[76] B. C. Vemuri and J. K. Aggarwal. Sensing 3-D Surface Using a Projected Grid. In *Proceedings of CVPR'86*, pages 602–607, Miami Beach, Florida, June 1986.

[77] P. Vuylsteke and A. Oosterlinck. 3D Perception with a Single Binary Coded Illumination Pattern. In *Proc. SPIE: Optics, Illumination and Image Sensing for Machine Vision*, volume 728, pages 195–202, October 1986.

[78] M. M. Wagner. *Core of the Burn-Injured Patient.* PSG Publishing Company, Littleton, 1981.

[79] M. W. Woolridge, N. Butte, K. G. Dewey, A. M. Ferris, C. Garza, and R. P. Keller. Methods for the Measurement of Milk Volume Intake of the Breast-feed Infant. In R. G. Jensen and M. C. Neville, editors, *Human Lactation: Milk Components and Methodologies*, pages 5–21. Plenum Press, New York and London, 1985.

[80] Y. Yakimovsky and R. Cunningham. A System for Extracting Three-Dimensional Measurement from a Stereo Pair of TV Cameras. *Computer Graphics and Image Processing*, pages 195–210, July 1978.